EFFECT OF VERTICALLY HETEROGENEOUS SOIL ON SIMULATED WATER STORAGE AND SURFACE ENERGY

A Thesis

by

JONATHAN WILLIAM GROSS

Submitted to the Office of Graduate and Professional Studies of
Texas A&M University
in partial fulfillment of the requirements for the degree of

MASTER OF SCIENCE

Chair of Committee,	Cristine L. S. Morgan
Co-Chair of Committee,	James L. Heilman
Committee Members,	Steven M. Quiring
	Haly L. Neely
Head of Department,	David D. Baltensperger

August 2017

Major Subject: Soil Science

ABSTRACT

The global effects of climate change and policy decisions are simulated, in part, by land surface models; yet, the models often use incomplete soil information that may result in unreliable estimates of soil water storage and surface energy fluxes. The objectives of this study were to: 1) quantify the impact of better representation of vertical heterogeneity of soil characterization on simulated soil water storage and surface energy fluxes; and 2) to simulate the effect of abrupt soil textural change from sandy to clayey (i.e. presence of argillic horizons) on patterns of simulated surface energy fluxes.

In this study, the Root Zone and Water Quality Model: Version 2 (RZWQM2) and measurements of soil moisture from soil in Palestine, TX (loamy, siliceous, semi-active, thermic Arenic Plinthic Paleudult) and Bronte, TX (fine loamy, mixed, superactive, thermic Typic Paleustalf) were used. The results showed that more accurate representation of vertical soil textural heterogeneity and hydraulic parameters improved the predictions of soil water storage compared to measurements. Simulations under an abrupt texture discontinuity, such as sandy over clayey soil, increased the magnitude of differences in latent and sensible heat partitioning. Additionally, accounting for a simulated argillic horizon revealed a predictable pattern of simulated latent heat fluxes as a function of claypan and rooting depths, where the interquartile range of latent heat fluxes: 1) shift to a maximum for claypans above the rooting depth, 2) plateau until the rooting depth, 3) shift to a minimum for claypans below the rooting depth, and 4) steadily increase shift with diminishing returns after the minimum has been reached.

This study showed that accurately simulating vertical changes in soil texture with depth changed estimates of plant available water and improved soil water prediction accuracy. Subsequently, simulated ranges of latent heat fluxes were also affected. Given improved reliability in simulation of soil water and latent heat fluxes in land surface models, the representation of soil vertical heterogeneity and hydraulic parameters are anticipated to improve the performance of land surface models.

DEDICATION

This thesis is dedicated to my father, mother, and sister.

Thank you for your love and support over the last decade.

CONTRIBUTORS AND FUNDING SOURCES

Contributors

This work was supported by a thesis committee consisting of Dr. Cristine L. S. Morgan (chair), Dr. James Heilman (co-chair), and Dr. Haly L. Neely of the Department of Soil and Crop Science and Dr. Steven Quiring of the Department of Geography.

The weather and soil moisture data analyzed for Chapter III were provided by the Climate Reference Network. The data quality was checked using an algorithm provided by Dr. Steven Quiring. The Root Zone and Water Quality Model Version 2 and model training used for this thesis was developed and provided by USDA ARS in Ft. Collins, CO.

All other work conducted for the thesis was completed by the student independently.

Funding Sources

Graduate study was supported by an assistantship from Texas A&M University and funding from the Texas Commission on Environmental Quality.

ACKNOWLEDGEMENTS

I would like to thank my committee chair, Dr. Morgan, and my committee members, Dr. Heilman, Dr. Quiring and Dr. Neely, for their guidance and support throughout the course of this research.

Thanks also go to my friends, colleagues and the department faculty and staff for making my time at Texas A&M University a great experience. I also want to extend my gratitude to Texas Commission on Environmental Quality for providing funding for the work and USDA ARS for assistance with Root Zone Water Quality Model for the study.

NOMENCLATURE

$\|\Delta SD\|$	Absolute difference between two standard deviations
AT	Actual Transpiration
AE	Actual Evaporation
Ψb or τb	Air Entry Pressure Potential (cm)
A180	Any RZWQM2 simulation initialized with measured soil textures and a maximum vegetation rooting depth of 180 cm
SC180	Any RZWQM2 simulation initialized with sand over clay soil textures and a maximum vegetation rooting depth of 180 cm
SC80	Any RZWQM2 simulation initialized with sand over clay soil textures and a maximum vegetation rooting depth of 80 cm
AWDN	Automated Weather Data Network
ρ_B	Bulk Density
τ_c	Capillary Suction Head (cm)
C:N	Carbon:Nitrogen Ratio
α and n	Characteristics of Van Genuchten Soil Water Release Curve
CRN or USCRN	United States Climate Reference Network
CLM	Community Land Model
CONUS	Contiguous United States
STATSGO	State Soil Geographic Database
T_s^t	Current Soil Surface Temperature (˚C)
DOY	Day of the Year
Θ	Degree of Saturation

z	Depth from Surface of a Point in Soil
Δlatent	Difference between two latent heat fluxes
Δsensible	Difference between two sensible heat fluxes
Δstorage	Difference between two soil water storages
DD	Deep Drainage
T_z^t	Expected Lower Boundary Soil Temperature (˚C)
SW	Extended Shuttleworth and Wallace Module
GHCN	Global Historical Climatology Network
Ψ_g	Gravimetric Pressure Potential (cm)
$\overline{K}_{sat}$	Harmonic Average of Saturated Hydraulic Conductivities down to a Soil Wetting Front (cm hr^{-1})
τ	Hydraulic Pressure Potential (cm)
D	Index of Agreement
LSM	Land Surface Model
λE	Latent Heat Flux (W m^{-2})
PMS	Latent Heat Flux due to Soil Evaporation (W m^{-2})
PMR	Latent Heat Flux due to Surface Residue (W m^{-2})
PMC	Latent Heat Flux due to Transpiration (W m^{-2})
CC	Latent Heat Flux Proportion Constant of Canopy Height
CS	Latent Heat Flux Proportion Constant of Soil Depth
CR	Latent Heat Flux Proportion Constant of Surface Residue Depth
Ψ_m	Matric Pressure Potential (cm)
MAE	Mean Absolute Error

$\bar{M}$	Mean of the Measured Data
$\bar{P}$	Mean of the Predicted Data
$\bar{\theta}$	Mean Volumetric Soil Water Content ($m^3\ m^{-3}$)
M	Measured Data
NSE	Nash-Sutcliffe Efficiency
NOAH-MP	NOAA, Oregon State University, Air Force, and Hydrology Lab Model with Multi-Parameterization Options
Rn	Net Surface Energy ($W\ m^{-2}$)
N	Net Water Balance
NASMD	North American Soil Moisture Database
n	Number of Predictions
Ψ_o	Osmotic Pressure Potential (cm)
PAW	Plant Available Water
P	Predicted Data
$T_s^{t-\Delta t}$	Previous Lower Boundary Soil Temperature (˚C)
Δz_s	Previous Soil Thickness (m)
QA/QC	Quality Assessment and Quality Control
RAE	Relative Absolute Error
θ_r	Residual/Hygroscopic Volumetric Soil Water Content ($m^3\ m^{-3}$)
RMSE	Root Mean Square Error
RZWQM2	Root Zone and Water Quality Model: Version 2
R	Runoff
K_s	Saturated Soil Hydraulic Conductivity ($cm\ hr^{-1}$)

θ_{sat}	Saturated Volumetric Soil Water Content ($m^3\ m^{-3}$)
H	Sensible Heat Flux ($W\ m^{-2}$)
SHAW	Simultaneous Heat and Water Model
K	Soil Hydraulic Conductivity ($cm\ hr^{-1}$)
λ, b	Soil Pore-Size Distribution Index
q	Soil Water Flow ($cm^3\ hr^{-1}$)
S	Soil Water Root Uptake ($m^3\ m^{-3}\ hr^{-1}$)
Z_{wf}	Soil Wetting Front Depth from Surface (cm)
SD	Standard Deviation
G	Subsurface Heat Flux ($W\ m^{-2}$)
V	Surface Water Infiltration Rate ($cm\ hr^{-1}$)
H_0	Surface Water Ponding Depth (cm)
k_s	Thermal conductivity of the soil ($W\ m^{-1}\ ^{\circ}K^{-1}$)
Δt	Timestep Duration (hr)
Ψ_t	Total Pressure Potential (cm)
USDA ARS	United States Department of Agriculture - Agriculture Research System
C_s	Volumetric Soil Heat Capacity ($J\ m^{-3}\ ^{\circ}K^{-1}$)
θ	Volumetric Soil Water Content ($m^3\ m^{-3}$)
θ_{FC}	Volumetric Soil Water Content ($m^3\ m^{-3}$) at Field Capacity
θ_{WP}	Volumetric Soil Water Content ($m^3\ m^{-3}$) at Wilting Point

TABLE OF CONTENTS

Page

LIST OF FIGURES

Page

LIST OF TABLES

Page

CHAPTER I

INTRODUCTION AND LITERATURE REVIEW

Introduction

Modeling the exchange of mass and energy in the natural environment requires accurate information about the physical properties of soil and vegetation, plus others. Biophysical models can simulate biophysical processes of a given location; however, modeled outcomes are only as good as the information representing soil and plant properties. Over broader areas, Land-Surface Models (LSMs) solve biophysical processes and are generally coupled with atmospheric models to answer questions of air quality and climate change. Large soil data sets, such as the Conterminous United States (CONUS) – State Soil Geographic (STATSGO) digital database (Miller and White, 1998), are used as inputs for LSMs. Although LSMs use the spatial location and textural class of the surface soil from these data sets, LSMs still poorly represent soil, which results in inaccurate water storage and energy flux simulation (Gochis et al., 2010).

One limitation of the use of soil information by LSMs is the representation of varied soil texture with depth. For example, the National Oceanic and Atmospheric Administration, Oregon State University, Air Force, Hydrology Lab Model with Multi-Parameterization Options (Noah-MP; Niu et al., 2011) and the Community Land Model (CLM; Lawrence et al., 2011), both use surface-soil textures from CONUS STATSGO, but assume a uniform soil texture from the surface to a constant depth for any soil at any

given location (Chen and Dudhia, 2001; Lawrence et al., 2011). This is a poor representation of soil because varied soil texture with depth exists extensively across the US and globally.

Varied soil texture with depth is important for approximating soil water storage (Gupta and Larson, 1979) and movement (Richards, 1931; Childs and Collis-George, 1950), accurately. Representing soil texture as uniform with depth, results in incorrectly accounting for soil water storage and related outputs. Therefore, adjusting LSMs to use varied soil textures with depth is expected to be key in improving soil water content simulation and, in effect, surface-energy flux simulation.

The ability to assess adjustments that influence LSM estimates would facilitate more understanding of how including a varied soil texture with depth might influence water and energy flux simulation. However, such assessment by using LSM simulation alone is complicated because of the complexity of an LSM model and because the LSM represent a very coarse spatial scale (1 km^2) and soil measurements for validation represent a smaller scale (1 m^2). A rigorous assessment using an LSM simulation requires a large data set of soil textures with associated soil moisture at depth, as well as soil and land use information across space.

An intermediate step for assessment, and the overall goal of this research, is to use a well-studied, well-used biophysical model that has been shown to better represent the knowledge of soil-water-plant interactions. A model such as the Root Zone Water Quality Model: Version 2 (RZWQM2; Ma et al., 2012) can be run for the 1 m^2 scale and allows

some assessment of how varying soil texture with depth would alter soil moisture storage and associated energy flux estimates.

Texas has substantial expanses of soils that change texture abruptly with depth, primarily from the translocation of clays to the subsoil. The translocation of clays from the soil surface, along with weathering of primary soil particles to clays, generally creates surface soil horizons that are low in clay content and illuvial horizons that are relatively finer. In some areas, particularly in Central and East Texas, this process is accentuated and creates conditions where there is an abrupt texture change from the surface or elluvial horizon to the illuvial horizon, forming the Texas Claypan Major Land Resource Area (Soil Survey Staff, 2006). Because the soil surfaces of claypan soils are sandy, and because the LSMs are assigning the surface texture to the whole profile, these claypan soils are getting assigned to be deep sandy soil, where in fact the sandy layer is only 20 to 100 cm deep with clay soil below. This variability can result in significant differences in water storage and surface energy partitioning.

The overall objective of this project was to determine the effect of accurate representation of vertical soil heterogeneity on selected biophysical model outputs. To achieve this objective, the RZWQM2 was used to simulate soil water storage, latent heat, and sensible heat fluxes with increased sensitivity to varied soil texture with depth than LSMs. The hypothesis tested is that a vertically heterogeneous representation of soil texture will improve simulation of soil water storage and energy fluxes. The specific objectives of this project were to 1) quantify the difference in model simulation results of soil moisture, latent heat, and sensible heat with a texturally homogenous and

heterogonous claypan soil in udic and ustic soil moisture regimes; and to 2) determine the effect of abrupt textural change with soil depth on patterns of surface-energy fluxes.

Claypan soils in East Texas receive about 113 cm of annual rainfall, whereas West Texas claypans receive less than 60 cm of annual rainfall. To address O**bjective 1**, water storage and movement was simulated in a soil under two different rainfall regimes using RZWQM2, which can assign variations in soil texture with depth. Simulation results were compared to measured values of soil moisture from two USCRN sites. Measured and simulated values of soil water content were compared using the relative absolute error (RAE), Nash-Sutcliffe efficiency (NSE), index of agreement (D), root mean squared error (RMSE), and linear regressions (Willmott, 1981; Moriasi et al., 2007; Bennett et al., 2013).

The RZWQM2 uses the Simultaneous Heat and Water (SHAW) module to simulate surface heat flux partitioning (Flerchinger and Saxton, 1989). To address O**bjective 2**, surface heat flux outputs were calculated by SHAW to determine if soils with similar environments and differing textural depths (e.g. varying the depths of a claypan soil) yield patterns of surface heat flux partitioning. If heat flux partitions were patterned, the causes of pattern fluctuations were determined by reviewing the range distributions of heat fluxes from simulations of increasing claypan depths.

Literature Review

Root Zone Water Quality Model: Version 2

The Root Zone Water Quality Model: Version 2 (RZWQM2) is a one-dimensional (1D) biophysical model developed by the United States Department of Agriculture in the Agriculture Research System (Ma et al., 2011). Capable of simulating mass and energy fluxes, pesticide and nutrient transport, plant growth, and crop management effects, RZWQM2 has been tested and widely used by the soil and biophysical modeling community (Starks et al., 2003; Fox et al., 2004; Fang et al., 2010). More importantly, the geometry of RZWQM2's mass and energy simulation of biophysical processes are similar to the geometry of the Noah-MP model (e.g. – soil, snow, and canopy layers).

RZWQM2 can calculate the soil water storage from rainfall, estimate the potential evapotranspiration at the soil surface, and simulate surface soil water and energy fluxes using soil texture and layer information and hourly weather records. Simulated soil water is solved using Richard's Equation for user-defined soil textures at varying horizon depths (Ma et al., 2011), while the Simultaneous Heat and Water (SHAW) module calculates hourly energy balance for the plant canopy and soil (Flerchinger and Pierson, 1991). Furthermore, RZWQM2 has been validated continuously over the last decade, since its inception in 1992, and continues to be updated and further validated by the biophysical modeling community (Hanson et al., 1998; D. N. Moriasi et al., 2012; Ma et al., 2012).

For these reasons, RZWQM2 was ideal for this project as it represents LSM processes, while allowing a focus on the soil component.

Soil Water in RZWQM

In the RZWQM2, hourly precipitation can become runoff, infiltrated soil water, redistributed soil water, evaporated, or transpired. Infiltration partitioning was calculated at the surface boundary condition Green & Ampt equation (Green and Ampt, 1911) of the form

$$V = \overline{K}_{sat}\left(\frac{\tau_c + H_0 + Z_{wf}}{Z_{wf}}\right), \quad \text{(Eq. 1)}$$

where V was infiltration rate (cm hr^{-1}), $\overline{K}_{sat}$ was effective average saturated hydraulic conductivity (cm hr^{-1}), τ_c was capillary suction head (cm), H_0 was ponding depth (cm), and Z_{wf} was wetting front depth (cm). If the surface-soil infiltration rate was faster than the rainfall rate for that hour, infiltration was set equal to the rainfall rate. If the rainfall rate was more than what surface-soil infiltration rate could conduct, excess water was partitioned as runoff. As water infiltrated each soil layer, the current soil layer and all overlying soil layers contributed to the harmonic mean of $\overline{K}_{sat}$, which improved runoff partitioning responsiveness to a sudden increase or decrease in clay content.

The current layer's water storage was calculated by the difference in initial water content and field capacity, referred to as the water deficit, after an infiltration rate was established for a soil layer. Then, the infiltration rate was used to "fill" the water deficit to

calculate the current layer's hourly time step. After waiting the time step, remaining infiltration moved to the next lower layer.

Vertical redistribution between soil layers was calculated for the current time step after the precipitation was partitioned as infiltration or runoff. Lateral redistribution did not occur with the tile drain functions turned off. Both the infiltrated water storage (θ) and the initialized soil hydraulic properties determined the pressure head (τ) used to calculate hydraulic conductivity (K). The volumetric water content and hydraulic conductivity relationship was calculated using the Brooks and Corey equation (Brooks and Corey, 1964) of the form

$$\begin{aligned} \theta(\tau) &= (\theta_{sat} - \theta_r)\left(\frac{\tau_b}{\tau}\right)^{\lambda} + \theta_r \quad \tau > \tau_b \\ \theta(\tau) &= \theta_{sat} \qquad\qquad\quad \tau \leq \tau_{b,} \end{aligned}, \qquad \text{(Eq. 2)}$$

and

$$\begin{aligned} K(\tau) &= K_{sat}\left(\frac{\tau_b}{\tau}\right)^{2+3\lambda} \quad \tau > \tau_b \\ K(\tau) &= K_{sat} \qquad\qquad \tau \leq \tau_b, \end{aligned}, \qquad \text{(Eq. 3)}$$

where θ was current water storage ($m^3\ m^{-3}$); θ_{sat} was saturated water content ($m^3\ m^{-3}$); θ_r was residual (i.e. – hygroscopic) water content; τ_b was air entry potential (cm); τ was hydraulic pressure head (cm); λ was pore size distribution index (unitless), K was hydraulic conductivity (cm hr^{-1}); and K_{sat} was saturated hydraulic conductivity (cm hr^{-1}). The hydraulic conductivity and pressure head were then referenced by a numerical redistribution solution (Richards, 1931) of the form

$$\frac{\partial \theta}{\partial z} = \frac{\partial}{\partial z}\left(K\frac{\partial \tau}{\partial z} - K\right) - S \qquad \text{(Eq. 4)}$$

where z was soil layer depth (cm) and S was root water uptake (hr^{-1}). Redistribution continued through numerically solved layers (nodes) down to the lower boundary conditions of the soil profile. A unit gradient was used at the lower boundary condition, which means that the hydraulic conductivity of the lowest layer and root water uptake governed how fast water left the profile.

In RZWQM2, actual evaporation and transpiration were computed by potential evaporation and root water uptake, respectively. Actual evaporation equaled potential evaporation when water remained at the soil surface. Once the surface pressure head was less than -20,000 cm, the surface pressure head was referenced for redistribution calculations. Actual transpiration was limited by potential transpiration as the maximum actual transpiration. Actual transpiration was governed by root water uptake. Potential evapotranspiration relied, significantly, on energy balance and was solved with the extended Shuttleworth and Wallace (SW) module. Evapotranspiration in the extended SW module (Farahani and Ahuja, 1996) followed the form

$$\lambda E = CC(PM_C) + CS(PM_S) + CR(PM_R), \quad \text{(Eq. 5)}$$

where λE was latent heat flux, CC, CS, and CR were proportion constants of the canopy, soil, and residue, respectively, for total latent heat flux, and PM_C, PM_S, and PM_R were transpiration, soil evaporation, and residue latent heat fluxes, respectively.

Energy Balance in RZWQM

In RZWQM2, the potential evapotranspiration and latent heat of vaporization of water (Eq. 5) represented the maximum allowed latent heat flux. Net radiation (R_n) minus the stored energy in the soil (G) was the energy available for latent (λE) and sensible (H) heat (van Bavel and Hillel, 1976), as shown in Eq. (18),

$$R_n = \lambda E + H + G. \quad \text{(Eq. 6)}$$

From this energy equation, soil, residue, and canopy temperatures are computed and iteratively balanced within SHAW.

The USCRN sites data included incoming radiation and relative humidity. This data was used to calculate λE and H, which left G as the remaining variable for solution. To solve G, RZWQM2 ran a simplified PENMAN flux model of soil temperature (Luo et al., 1992) of the form

$$G = \frac{k_s(T_s^t - T_z^t)}{\Delta z_s} - \frac{C_s(T_s^t - T_s^{t-\Delta t})}{2\Delta t}, \quad \text{(Eq. 7)}$$

where k_s was thermal conductivity of the soil (W m-1 K-1); T_s^t was the current soil surface temperature (˚C); T_z^t was expected lower boundary soil temperature (˚C); Δzs was soil thickness of the time step (m); Cs was volumetric heat capacity of soil (J m-3 K-1); $T_s^{t-\Delta t}$ was the previous time step's soil surface temperature; and Δt was the time step duration (s). The SHAW module was in non-wintering mode because snow was not simulated at either site. To ultimately calculate G, the various soil temperatures was calculated by solving the canopy temperatures first, followed by the residue temperatures, and finally,

the soil temperatures were numerically computed to convergence for each node. Solving G allowed the energy equation to be balanced within the SHAW module.

Soil Physical Property Tables

RZWQM2 primarily depends on an estimate of water content (θ) at saturation (θ_{sat}), field capacity, permanent wilting point, and air-dry (θ_r) along with a slope and intercept of the soil moisture retention function as input soil parameters. These parameters can be obtained from a look-up table based on soil texture class (Gupta and Larson, 1979; Rawls et al., 1982, 1998; Saxton et al., 1986; Saxton and Rawls, 2006). Property tables are sets of hydraulic properties for generic soil textures. The earliest table is the Rawls et al. (1982) table, which compiled USDA soil sample properties from across the CONUS to generate mean water retention properties, bulk densities, air entry potentials, and hydraulic conductivities by soil texture class. The Rawls et al. (1982) table has water retention values that were estimated with Gupta and Larson (1979) regressions using CONUS sand, silt, clay, organic matter, and bulk density measurements. Porosities and air entry potentials were estimated from regression of saturation versus hydraulic conductivity CONUS data and confirmed with Brutsaert equations (Brutsaert, 1967).

While CONUS data were useful in creating a seminal table for input into LSMs and biophysical models, the Rawls table provides averaged CONUS values by soil texture class and lacks spatially explicit application. To improve application, pedotransfer functions aimed to continuously calculate soil properties based on clay and sand contents

(Saxton et al., 1986), and later, organic matter as well (Saxton and Rawls, 2006). However, these more continuous types of pedotransfer function are not used in LSM models, whereas all soil properties are obtained from texture class. Still, much work remains to improve global and localized land surface modeling and remove dependence categorical pedotransfer tables.

Latent and Sensible Heat

After soil water is simulated based on the soil property table, energy flux is modeled. The net radiation as energy stored underground and emitted energy at the surface is represented by

$$R_n = \lambda E + H + G, \qquad \text{(Eq. 8)}$$

where R_n is net radiation, λE is latent heat flux, H is sensible heat flux, and G is subsurface energy flux (van Bavel and Hillel, 1976). Emitted surface energy fluxes are partitioned into latent heat and sensible heat, while energy stored from incoming radiation is partitioned to subsurface heat.

Latent heat (λE), thermodynamically, is defined as the energy needed to evaporate water from a surface. Within the context of RZWQM2, λE is the energy emitted from water evaporation at the simulated surface, be it from soil, ponding, or from stomatal openings in vegetation. Sensible heat (H) is the thermodynamic energy associated with temperature fluxes in a medium. Within the context of RZWQM2, H is the emitted energy flux associated with changes in air temperature at the soil surface and in the plant canopy

above the soil. Subsurface heat (G) is the remaining energy not emitted at the land surface. Within the context of RZWQM2, G is associated with the thermal conductivity of a soil at a specific depth that vertically transmits energy from that depth toward an adjacent depth of lower energy. Alternatively, the specified depth may accept G from an adjacent depth of high energy.

Latent and sensible heat fluxes are important solutions within RZWQM since they indicate surface energy flux partitioning associated with water and temperature changes at the simulated surface. Therefore, assessing the impact of layered soil texture does not stop with assessing differences in soil moisture, because it is important to know how the energy fluxes are affected by homogeneous and heterogeneous soil moisture scenarios in RZWQM2, as well. The sensible and latent heat partitioning is important to understand as these simulated data are the desired end-product from the LSM models.

Claypans

Claypans are soil horizons of high clay accumulations under low-clay soil horizons. Various types of claypans can result from different soil genesis processes. Claypans resulting from weathering of primary minerals to silicate clays and translocation of clays are illuvially-derived forming 1) electrolyte pans and 2) attraction pans (Smith, 1934; Jenny and Smith, 1935).

Electrolyte pans can form in arid-humid transition zones from infrequent and intense rainfalls weathering soluble surfaces. Soil water, high in electrolytes, initially

makes clay particles immobile. As electrolyte concentrations drop, clay moves down the soil profile with soil water until salt horizons flocculate the clay forming a claypan. Small pores developed from the forming claypan mechanically catch other aggregated clays augmenting the claypan's development.

Attraction pans can form in humid and temperate climates from frequent rain weathering. Weathering translocates iron and aluminum cations down the soil profile to accumulate on negatively charged quartz grains. Excess cation charges attract negatively charged clay particles during clay illuviation. Protective surface vegetation accentuates the abruptness of the forming claypan.

Once these claypans form, the downward progression of water behaves differently from most other soils. The contrast of sandy over clayey soil combines two contrasting soil water storage capacities along with contrasting hydraulic conductivities to create rapid decreases in infiltration rates during storms, as well as, increased surface and subsurface runoff above and at the sand-clay boundary (Jamison and Thornton, 1961; Saxton and Whitaker, 1970; Doolittle et al., 1994; Blanco-Canqui et al., 2002). Consequently, plant growth and thermal energy storage are also affected by low surface water storage and high subsurface water storage creating a unique dynamic between incoming solar radiation and the energy emitted from the claypan soil.

CHAPTER II

MATERIALS AND METHODS

This project used RZWQM2: a 1D, biophysical model that uses soil, weather, crop, and management data to simulate mass and energy fluxes while accounting for water and nutrient transport and plant growth with the option of using custom soil textures and horizon depths (Ma et al., 2011). Hourly weather (forcing) data from the U.S. Climate Reference Network (USCRN) records was used for simulations and to initialize RZWQM2, and USCRN site data, such as vegetation type and soil texture were also used. The model was not calibrated in this study to avoid masking the effect of the soil information. Minimal initialization of soil hydraulic properties without calibration has been shown to provide accurate soil moisture dynamics (Starks et al., 2003) and will allow the results to be comparable to those found by running a LSM, such as Noah-MP.

Study Sites

Two USCRN sites in Texas were selected to address the project objectives. The first site was in East Texas (Palestine; 31.779367°, -95.723251°) and represents an udic soil moisture regime. The second site was near West Texas (Bronte; 32.040908°, -100.249513°) and represents an ustic soil moisture regime. An udic soil moisture regime is characterized as dry for less than 90 cumulative days for the top 50 cm of the argillic (illuvial-clay B horizon); whereas, an ustic soil moisture regime is normally dry for more

Figure 1. Soil and weather instrument at the Palestine, TX site (Bell, et al., 2013; Diamond, et al., 2013).

than 90 cumulative days and moist for more than 180 cumulative days for the top 50 cm of the argillic (Soil Survey Staff, 2014).

Palestine

At the Palestine site (Fig. 1), a Lilbert loamy fine sand is mapped and classified as a loamy, siliceous, semi-active, thermic Arenic Plinthic Paleudult (Soil Survey Staff, 1999). Lilbert is associated with 0-3% slopes with a loamy fine sand surface to 10 cm followed by a fine sandy loam argillic horizon that increases in clay content to a sandy clay loam at depth (Table 1). The vegetation associated with Lilbert is Common Bermudagrass and Lovegrass as the dominant vegetation (Soil Survey Staff, 2013). Common Bermudagrass [*C. dactylon*] grows to 30 to 60 cm in height at maturity and can have a maximum rooting depth of 2.5 m; though, deeper roots have been observed (Burton, et al., 1954). Common Bermudagrass can have a maximum leaf area index of 2.20 (Kiniry, et al., 2007).

Table 1. Particle size distribution for the soil profile at the Palestine, TX site (Bell et al., 2013).

Palestine, TX Site Properties				
Horizon Depth	Soil Texture	% Sand	% Silt	% Clay
5 cm	Loamy Fine Sand	81	16	3
10 cm	Loamy Fine Sand	78	15	7
20 cm	Fine Sandy Loam	74	8	18
50 cm	Sandy Clay Loam	73	5	22
100 cm	Sandy Clay Loam	75	5	20

Bronte

At the Bronte site (Fig. 2), the soil is mapped as Miles fine sandy loam which is classified as a fine loamy, mixed, superactive, thermic Typic Paleustalf (USDA-NRCS, 2014a). The soil was associated with 1-3% slopes with a fine sandy loam surface to 20 cm that abruptly increased in clay content to a sandy clay loam at depth (Table 2). The vegetation associated with this soil is Little Bluestem, Switchgrass, and Blue Grama as the dominant vegetation (USDA-NRCS, 2014b). While Common Bermudagrass did not dominate the site, Common Bermudagrass did grow in Bronte and had similar properties

Figure 2. Soil and weather instrument at the Bronte, TX site (Bell, et al., 2013; Diamond, et al., 2013).

Table 2. Particle size distribution for the soil profile at the Palestine, TX site (Bell, et al., 2013).

Bronte, TX Site Properties				
Horizon Depth	Soil Texture	% Sand	% Silt	% Clay
5 cm	Fine Sandy Loam	76	12	12
10 cm	Fine Sandy Loam	76	13	11
20 cm	Fine Sandy Loam	74	12	14
50 cm	Sandy Clay Loam	59	10	31
100 cm	Sandy Clay Loam	61	9	30

to that of Blue Grama [*B. gracilis*]. Blue Grama grows from 30 to 60 cm in height (Ares, 1976) and can have a maximum rooting depth of 3 m (Ares, 1976). Blue Grama can have a maximum leaf area index from 0.6 to 1.0 (Ares, 1976).

Data and Instrumentation

The USCRN sites collect soil and weather data hourly, convert it to daily and monthly formats, and publicly store: ftp://ftp.ncdc.noaa.gov/pub/data/USCRN/products. Wind speed data are collected at 5-minute intervals. Each site has collected data on the weather and soil (Diamond et al., 2013; Bell et al., 2013). Weather is collected 1.5-m above the ground and included air temperature and relative humidity, shortwave radiation, wind speed, and precipitation. Soil moisture and temperature are measured, in triplicate, using a Stevens Hydra Probe II Soil Sensor Model SDI-12 (Stevens Hydra Probe II Soil Sensor Model SDI-12) at 5, 10, 20, 50, and 100 cm deeps (Seyfried et al., 2005).. Dielectric readings from three sets of soil probes are averaged (Bell et al., 2013). The

manufacturer calibration (for sand, silt, or clay) is used to convert dielectric to soil moisture, the soil moisture probes were not calibrated to the soil found at each site (Seyfried et al., 2005; Bell et al., 2013).

Missing data were found in CRN weather data. Missing data from 1 to 5 hr in duration were interpolated using a spline. Any missing data more than 6 hr in duration were patched with temporally local data, which did not occur more than three times per weather data set. For quality control, soil moisture data were run through the North American Soil Moisture Database (NASMD) procedure (Quiring et al., 2015). The NASMD procedure was developed similarly to the algorithms used successfully by the Oklahoma Mesonet, West Texas Mesonet and Automated Weather Data Network. The algorithm includes tests for soil moisture range, persistence, magnitude, and variability. No additional adjustments were made to the soil moisture data.

Scenario Development

Each soil, or site location, was set up as an individual project within RZWQM2. The scenario start and stop times were set to January 1, 2009 and June 23, 2014, respectively. Four subroutines in the RZWQM2 were initialized per scenario: site description, initial state, residue state, and management practices. The entire "initial state" subroutine was set to default settings. Settings for the other three subroutines are described below.

Site Description

A scenario's site description included general information, horizon description, soil hydraulics, soil physical properties, hydraulic control, background chemistry, potential evapotranspiration, nutrients, and ammonia. Default parameters were used for the soil physical properties, hydraulic control, background chemistry, nutrients, or ammonia. Under potential evapotranspiration, default settings were used except the SHAW module was turned on so that detailed energy balance outputs would be available. The general site information used area, elevation, aspect, latitude, longitude, slope, and climate zone for all scenarios. Climate zone options are 1, 2, or 3, where each setting represents "less than 10", "between 10 and 20", or "greater than 20" inches of rainfall per year, respectively. Palestine scenarios were set to 1 ha, 115.8 m in elevation, 281.25º aspect, 31.78º latitude, -95.72º longitude, 6.74º slope, and climate zone 3. Bronte scenarios were set to 1 ha, 608.69 m in elevation, 135º aspect, 32.04º latitude, -100.25º longitude, 0º slope, and climate zone 2.

The horizon descriptions changed between sites because the soil profiles are different as well the horizon descriptions varied according to objectives. To meet the first objective, scenarios included a texturally homogeneous and heterogeneous soil profiles for each location. Homogeneous scenarios for Palestine projects were set to five horizons of loamy sand, whereas heterogeneous scenarios used textures from Table 1. Homogeneous scenarios for Bronte projects were set to five horizons of sandy loam,

whereas heterogeneous scenarios used textures from Table 2. All of these scenarios used horizon depths at 5, 11, 20, 50, and 200 cm.

For the second objective, both the depth of the argillic horizon and the rooting depth of the plant were altered for both sites (Palestine and Bronte). Horizon textures started with homogenous clay for scenario 1, and then 5 cm of sand was added to the surface with subsurface clay to 200 cm (Scenario 2). For Scenario 3, the surface depth of sand was 10 cm and then increased for subsequent scenarios by 10 cm, resulting in 22 total scenarios, where the last scenario is homogenous sand to 200 cm (see Table 3 for an illustration). Additionally, rooting depth was altered, the project labeled SC180 represent the 22 scenarios with Bermudagrass rooting to 180 cm, and SC80 uses the 22 scenarios with and a maximum rooting depth or 80 cm. Additionally the 22 scenarios were also simulated for each location, but using the measured texture classes (Tables 1 and 2) and

Table 3. Scenarios 9 and 10 demonstrate the 10 cm incremental increase in claypan depth for sand over clay scenarios.

Node	Horizon Depth	Texture	Horizon Depth	Texture
	Scenario 9		*Scenario 10*	
1	20 cm	Sand	20 cm	Sand
2	40 cm	Sand	40 cm	Sand
3	60 cm	Sand	60 cm	Sand
4	70 cm	Clay	80 cm	Clay
5	100 cm	Clay	100 cm	Clay
6	120 cm	Clay	120 cm	Clay
7	140 cm	Clay	140 cm	Clay
8	160 cm	Clay	160 cm	Clay
9	180 cm	Clay	180 cm	Clay
10	200 cm	Clay	200 cm	Clay

Table 4. Soil hydraulic properties used for RZWQM2, adapted from Kishné et al. (2017).

Soil Texture	K	θ_{sat}	θ_{FC}	θ_{WP}	θ_{R}	ρ_{B}
	$cm\ hr^{-1}$	---------- $m^3\ m^{-3}$ ----------				$g\ cm^{-3}$
Sand	8.640	0.402	0.086	0.024	0.004	1.585
Loamy Sand	6.192	0.396	0.142	0.057	0.010	1.601
Sandy Loam	3.636	0.413	0.213	0.081	0.016	1.556
Sandy Clay Loam	2.549	0.416	0.288	0.168	0.029	1.548
Clay	0.598	0.506	0.428	0.285	0.058	1.309

altered their depths (A180). The rooting depth for A180 was set to 180 cm. Each scenario used all 10 available nodes in RZWQM2, for solving the water balance. Look up, soil hydraulic properties were assigned by texture class using the custom hydraulic table developed for Texas soil textures (Kishné et al., 2017; Table 4).

Residue State

A scenario's residue state specifies initial residue, inorganic nitrogen, and surface residue properties. Surface residue properties were left at default settings. Initial residue and inorganic nitrogen were estimated with the initialization wizard guided by recommended settings. For Palestine, each soil horizon simulated 0.1% organic matter (580 $\mu g_{organic\ carbon}\ g_{soil}^{-1}$), default organism counts (474.5 $\mu g_{organic\ carbon}\ g_{soil}^{-1}$), 20% humus in fast and intermediate decomposition pools (94.9 $\mu g_{organic\ carbon}\ g_{soil}^{-1}$), and 80% humus

in fast decomposition pool (75.9 $\mu g_{organic\ carbon}\ g_{soil}^{-1}$). For Bronte, the same values as Palestine were used, except 20% humus in fast decomposition pool (19.0 $\mu g_{organic\ carbon}\ g_{soil}^{-1}$). The difference between fast decomposition pools was based on each site's vegetation conditions. Palestine has more vegetation and soil organics; whereas, Bronte has less.

Management Practices

A scenario's management practices were defined by crop selection, crop planting methods, manure, irrigation, fertilization, pesticides, and tillage. Manure, irrigation, fertilizer, pesticides, or tillage practices were not simulated for either project, which left crop selection and planting methods to initialize. The QuikTurf module was used to initialize the crop physiology for grasses. QuikTurf is a simplified plant growth plug-in that maintains a zero-mass, constant rooting depth and increases LAI and plant height linearly from each turf trimming to a maximum growth. The root distribution fraction is a linear function of the planting method depth and the maximum root depth.

Bermudagrass settings were initialized for both projects, but grass physiology was altered based on maximum rooting depth at 180 and 80 cm (Table 5), as described for the second objective scenarios. In objective one, homogeneous and heterogeneous scenarios used 180 cm rooting depths. Beginning March 15, 2009, all simulations simulated planting 40.5 million seeds with 1 cm row spacing at 1 cm depths. The turf was harvested June 17, 2014 with 5 cm stubble and at 100% harvest efficiency.

Table 5. QuikTurf module settings for common Bermudagrass used in both Palestine and Bronte projects' scenarios.

Dormancy DOY	Cutting DOY	Maximum Rooting Depth	Turf Height			Turf Leaf Area Index		Stover		Dead Roots		Total N Uptake
			Initial	Pre-cut	Post-cut	Pre-cut	Post-cut	Post-cut	C:N	Post-cut	C:N	
		---------- cm ----------				---- cm^2 cm^{-2} ----		kg ha^{-1}		kg ha^{-1}		kg ha^{-1}
77	289	180 (normal)	11.66	45	5	2.2	0	1000	40	0	40	50
		80 (stunted)	11.66	22.78	5	1.31	0	444.44	40	0	40	22.23
1	1	30 (default)	20	20	10	20	2.5	2000	50	0	50	50

Statistical Methods

Recommended quantitative metrics and visual aids were used to analyze the hydrology outputs (Moriasi et al., 2007; Ma et al., 2012; Bennett et al., 2013) of RZWQM2 and determine the effects of textural hetero- versus homogeneity on soil water and surface heat fluxes. The effects of texture on θ predictions generated by RZWQM2 are assessed with their means, standard deviations (SD), bias, root mean square errors (RMSE), mean absolute errors (MAE), Nash-Sutcliffe efficiencies (NSE; Nash and Sutcliffe, 1970), relative absolute errors (RAE), and index of agreements (D; Willmott, 1981). The calculations for bias, RMSE, MAE, NSE, RAE, and D are defined by:

$$bias = \sum(P - M)\ /n, \quad \text{(Eq. 9)}$$

$$RSME = \sqrt{\sum(P - M)^2\ /n}, \quad \text{(Eq. 10)}$$

$$MAE = \sum|P - M|\ /n, \quad \text{(Eq. 11)}$$

$$NSE = 1 - [\sum(P - M)^2\ / \sum(M - \bar{M})^2], \quad \text{(Eq. 12)}$$

$$1 - RAE = 1 - [\sum|P - M|\ / \sum|M - \bar{M}|] \text{ and} \quad \text{(Eq. 13)}$$

$$D = 1 - [\sum(P - M)^2\ / \sum(|P - \bar{M}| + |M - \bar{M}|)^2], \quad \text{(Eq. 14)}$$

where P are predicted and M are measured values, and $\bar{P}$ and $\bar{M}$, are the averages of n predictions and measurements, respectively. Other metrics like totals, mean lines, medians, ranges, and quartiles were transformed into visual aids, such as continuous box plots, linear regressions, and time series.

Soil Water Metrics

The $\bar{\theta}$ of the heterogeneous- and homogeneous-texture simulations are contrasted with the measured $\bar{\theta}$. The standard deviation (SD) and bias (Eq. 9) statistics represent RZWQM2 θ prediction variation and shift about the measured $\bar{\theta}$, respectively. The RMSE (Eq. 10), which is a commonly utilized statistic in hydrology verification techniques, will be complimented by the MAE's (Eq. 11) lessened sensitivity to extreme differences. This is important so that the effects of extreme deviations of RZWQM2 predictions from the measured θ are understood. The MAE and RMSE have additional utility because they express predicted error in the same units as the measured data, which improves our comprehension of the statistics.

The unitless indices of NSE (Eq. 12), RAE (Eq. 13) and D (Eq. 14) compare RZWQM2 θ prediction trends using the trend of the measured $\bar{\theta}$ as the minimal model for acceptance. The NSE, also referred to as R^2, ranges from negative infinity to one. According to Bennett et al. (2013), any negative NSE should be interpreted as if the linear trend of the measured $\bar{\theta}$ is a better predictor of θ than a hydrologic model's predictions of θ. At zero, the RZWQM2 trend of θ predictions would be the same as the trend of the measured $\bar{\theta}$ as a model for predicting θ. An NSE of one means the simulated predictions and measured θ are comparable. Taking after Nash and Sutcliffe (1970), L. Ma et al. (2012) considers NSE as the relationship between model error and the scatter of measured data where an NSE of 0.7 is minimally acceptable for RZWQM2. Both perspectives are considered.

The NSE, a commonly used hydrology verification statistic, will be complimented by the other unitless indices RAE, used as $1 - RAE$ in this project because it has the same index range and meanings as the NSE (Bennett et al., 2013), and Willmott's D-index, which ranges from zero to one where zero is bad, 0.7 is minimally acceptable, and 1 is perfect trend simulation of the measured θ for RZWQM2 (Ma et al., 2011). The RAE is less sensitive to extreme differences between simulated and measured θ and will act as a baseline of trend error; whereas, NSE and D are more sensitive and will be more descriptive of how the trend is affected by large errors. The D index provides added utility because it is forgiving to predictions with better trends and increased systematic bias (Willmott, 1981). To reiterate and summarize the unitless indices, $1 - RAE$ will be a baseline for the NSE, then D will be compared to $1 - RAE$ and NSE to evaluate overall trend prediction. The RAE is represented as $1 - RAE$ to simplify the index comparisons by setting its ideal value to one and its unacceptable values to zero or less.

The visual aids use mean lines and compare ranges, medians, and interquartile ranges in the form of time series and linear regressions. Multiple time series plot the weekly interquartile ranges of homogeneous and heterogeneous simulated θ with the measured θ at 5, 10, 20, 50, and 100 cm depths throughout 2012. Another time series depicts the differences in profile water storage, latent heat fluxes, and sensible heat fluxes between the heterogeneous and homogeneous simulations. The linear regressions compare predicted surface heat fluxes between the heterogeneous and homogeneous simulations.

Partitioning and Sensitivity Analyses

The sensitivity of latent and sensible heat fluxes to abrupt changes in texture followed by a change in rooting depth was tested with linear regressions, average monthly evaporative fraction, water balance partitioning, and claypan depth versus latent heat flux graphs. The sensitivity analyses used the simulated heat flux data from the daylight hours only. The water balance partitioning uses continuous data because it is cumulative by necessity.

The average monthly evaporative fraction, a ratio that expresses the proportion of surface energy attributed to evapotranspiration, was plotted as a time series from 2011 to 2013. The evaporative fraction time series compared the simulated surface energies from 5, 20, and 100 cm deep claypans, side-by-side, from A180, SC180 and SC80 scenarios during 2011, 2012, and 2013.

The water balance partitions are depicted as bar charts for 2011, 2012, and 2013 summers for A180, SC180, and SC80 for the 5, 20, and 100 cm deep claypan scenarios for each site project. A summary table was then generated that depicted the net difference in available water partitioning from A180 to SC180 (texture change effects) and from SC180 to SC80 (root depth change effects). Available water was calculated as total soil column water minus the total summer precipitation. Available water was partitioned as runoff, actual transpiration, actual evaporation, or deep drainage.

Claypan depth vs heat flux graphs detailed how the range of latent heat flux changes as claypan depths increased with each successive simulation. Graphs were

generated using the ranges of latent heat from 22 SC80, 22 SC180, and 22 A180 scenarios during 2011, 2012, and 2013 from June through September. The ranges showed the minimum, maximum, median, and interquartile range of latent heat on a log scale. These graphs revealed the relationships, if any, of latent heat with soil textural changes.

CHAPTER III

RESULTS AND DISCUSSION

Effects of Textural Heterogeneity on Simulated Soil Water and Energy Fluxes

Soil Water Output and Metrics

The initialized scenarios for Palestine and Bronte were computed with heterogeneous and homogeneous soil profiles. The RZWQM2 generated daily soil water content (m^3 m^{-3}) for each scenario. Figures 3 and 4 show the weekly interquartile range of the measured and simulated soil water contents over 52 weeks starting January 1, 2012 for Palestine and Bronte, respectively. The weekly interquartile range represents the middle 50% of the data. There are five depths for each plot; each representing the depth of the soil moisture probes. The dashed horizontal lines represent the field capacities and permanent wilting points provided for that depth by the look-up table (Table 4). In general, the range of water contents exceeded the range of look-up table values for field capacity and wilting point. Based on plant available water (PAW) calculated using the look-up table, measured water contents at Palestine were within the PAW range of the look-up table except at 20 and 100 cm depths. At Bronte, the only measured mean water contents within the PAW range of look-up table, were at 20 and 50 cm depths.

Palestine, TX

For the loamy sand surface at 5 cm, heterogeneity and homogeneity simulations overestimated θ by 0.005 and 0.026 m^3 m^{-3}, respectively (Table 6). The heterogeneity simulation was closest to the measured θ values for most of 2012 with some overestimation in the summer and early winter. The heterogenous simulation was further from measured θ than homogeneous during drier conditions in late winter, spring, and the week 40 wetting period (Figure 3). However, homogeneous θ varied from measured θ ($|\Delta SD|$ = 0.045 m^3 m^{-3}) less than heterogeneous ($|\Delta SD|$ = 0.053 m^3 m^{-3}). The homogenous simulation also had the lower errors (MAE = 0.062 m^3 m^{-3}, RMSE = 0.071 m^3 m^{-3}) compared to heterogeneous (MAE = 0.065 m^3 m^{-3}, RMSE = 0.076 m^3 m^{-3}). This suggests the prediction and variation of θ was simulated better assuming homogeneous soil texture.

The results for the loamy sand at 10 cm were similar to the layer above it. There was little difference between the simulations, but homogenous outperformed heterogeneous slightly, by 0.03 m^3 m^{-3}. The D index suggests that both models were acceptable predictors of trend. Looking at both the 5 and 10 cm time series, we can see that there is some systematic bias associated with the heterogeneity simulation because predicted θ tended to be shifted drier to stay within the bounds of θ_{FC} and θ_{WP} for sandy loam, while the same predictions under homogeneity frequently wet above θ_{FC}. The week 40 wetting event at this depth showed a rapid increase in wetness for both simulations; however, the narrow range of PAW prevented an accurate representation. The simulated dry down phase was not as rapid as the measured dry down.

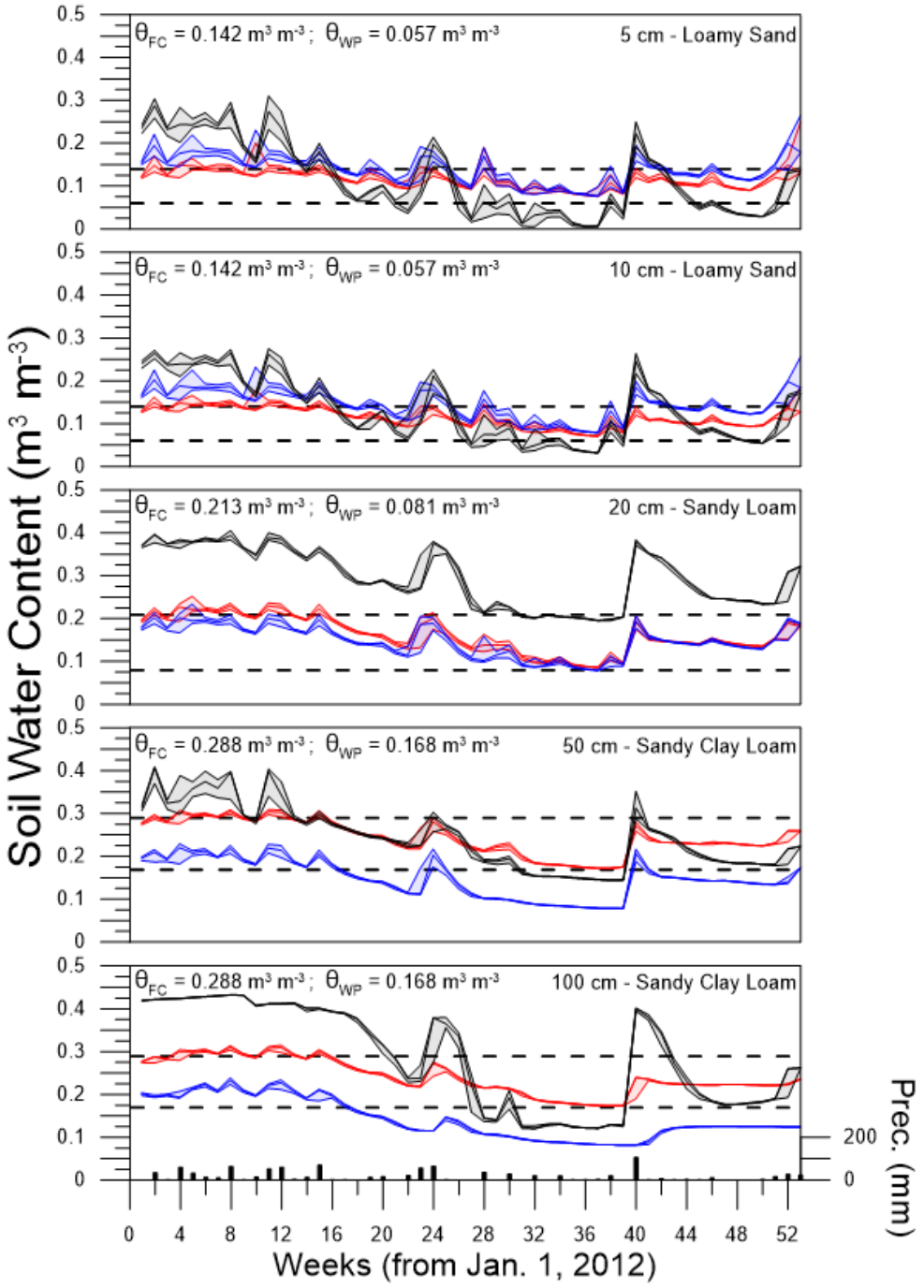

Figure 3. Modeled versus measured weekly soil water contents for a Lilbert loamy fine sand in Palestine, TX. Weekly water contents indicate the interquartile ranges and medians for measured (black), simulated homogeneous (blue), and simulated heterogeneous (red) soil profiles at five depths. Weekly precipitation totals are on the x-axis.

At 20 cm, the Palestine soil texture changes to a sandy loam, but the simulation of textural homogeneity maintains the hydraulic properties of the loamy sand (Table 4). Also, a systematic bias is because of the high measured θ that is inconsistent with the reported soil texture for CRN's probe at this depth. Both simulations had bias, MAE and RMSE values greater than $|0.13\ m^3 m^{-3}|$, as well as, negative 1-RAE and NSE values. For both SD and the D index, heterogeneity ($|\Delta SD|$ = 0.021 m^3 m^{-3}; D = 0.85) outperformed homogeneity ($|\Delta SD|$ = 0.025 m^3 m^{-3}; D = 0.84), which means the texture change simulated under a heterogeneous scheme improved the variation and trend of simulated θ. Importantly, the simulated change in texture would not be characterized as a claypan, yet the minimal improvement to water redistribution is still noticeable. Also, the week 40 wetting period was simulated similarly for both heterogenous and homogeneous soil textures.

At 50 cm the sandy clay loam claypan, or argillic layer, is present. Except for SD, all metrics for heterogeneous simulation indicate better prediction. The bias of the heterogeneous simulation was a sixth of homogenous simulation, while the MAE and RSME were a third. The D-index still indicated heterogeneous soil texture trended better than homogeneous (ΔD = 0.06), while neither simulation modeled the wetness of the first and last several months of 2012. Using a heterogeneous texture had the cumulative effect of improving simulation accuracy of θ as well as redistribution of water to lower layers.

At 100 cm, the soil is still a sandy clay loam, but simulated as a loamy sand under the homogeneous scheme. Again, there is obvious systematic bias in the homogeneous simulation and is evidenced by its increased error metrics and negative 1-RAE and NSE.

Table 6. Statistical summary of heterogeneous and homogeneous-simulation results for soil water content at Palestine, TX.

Soil Water Content Source	Profile Depth	$\bar{\theta}$	SD	$\lvert\Delta SD\rvert$	Bias	MAE	RMSE	1-RAE	NSE	D
	cm	---------- $cm^3\ cm^{-3}$ ----------								
Measured Heterogeneous Profile	5	0.12	0.089	-	-	-	-	-	-	-
	10	0.14	0.076	-	-	-	-	-	-	-
	20	0.3	0.069	-	-	-	-	-	-	-
	50	0.25	0.075	-	-	-	-	-	-	-
	100	0.29	0.12	-	-	-	-	-	-	-
Heterogeneous Profile	5	0.12	0.036	0.053	**0.005**	0.065	0.076	0.16	0.27	0.66
	10	0.12	0.031	0.045	-0.016	0.048	0.060	0.27	0.38	0.84
	20	0.17	0.048	**0.021**	**-0.13**	**0.13**	**0.14**	**-1.1**	**-2.9**	**0.85**
	50	0.25	0.042	0.033	**-0.001**	**0.03**	**0.039**	**0.51**	**0.72**	**0.95**
	100	0.24	0.042	0.075	**-0.044**	**0.081**	**0.092**	**0.25**	**0.38**	0.77
Homogeneous Profile	5	0.15	0.044	**0.045**	0.026	**0.062**	**0.071**	**0.19**	**0.36**	**0.83**
	10	0.15	0.043	**0.032**	**0.015**	**0.046**	**0.054**	**0.31**	**0.5**	**0.9**
	20	0.15	0.044	0.025	-0.14	0.15	0.15	-1.3	-3.8	0.84
	50	0.15	0.047	**0.027**	-0.096	0.096	0.1	-0.56	-0.89	0.89
	100	0.14	0.048	**0.069**	-0.14	0.14	0.16	-0.32	-0.97	**0.79**

† $\bar{\theta}$ is annual mean soil water content; $\lvert\Delta SD\rvert$ is the absolute difference between measured and simulated SD; MAE is mean absolute error; RAE is relative absolute error; and D is Willmott's index of agreement (1982).

‡ Bold numbers indicate better overall simulation of measured data.

However, the homogeneous predictions match the range of water contents better than the heterogenous, thus variation and trend metrics are better than heterogenous. However, the rate of redistribution of the measured θ is more rapid than measured. The homogenous simulation did not represent the rate of dry down well, nor the week 30 wetting event. Therefore, the heterogeneity simulation improves θ prediction over the homogeneity scheme.

Overall, three patterns in θ emerged from simulating Palestine soil heterogeneously versus homogeneously. First, the heterogeneity simulation of θ at the surface was comparable to the homogeneity simulation because the soil textures are the same under both schemes. Secondly, the improvement in increased clay content lower in the profile had a cumulative effect on redistribution toward deeper layers which resulted in improved θ predictions. Finally, the vertical heterogeneity of wilting points introduces systematic shifts in simulated θ. The resulting patterns indicate that heterogeneous simulation of soil texture improves the simulation of θ and redistribution as depth increases. Most importantly, the improvements were noticeable above the claypan, as well, indicating potential utility beyond Palestine's claypan heterogeneity, such as soils with less abrupt argillics.

Bronte, TX

At Bronte, TX, the surface was a sandy loam and both heterogeneous and homogeneous simulations both overestimated θ, especially during dry periods, by about 0.044 and 0.047 m^3 m^{-3} (Table 7), respectively. Both simulations remained within the bounds of the plant available water (0.08 m^3m^{-3} < θ < 0.21 m^3m^{-3}) for a sandy loam revealing both had a wilting point higher than that measured in the soil. The measured θ was more accurately represented by the heterogeneous simulation with lower errors (MAE = 0.045 m^3 m^{-3}, RMSE = 0.054 m^3 m^{-3}), whereas the homogeneous simulation had a closer range in variability (|ΔSD| = 0.0025 m^3 m^{-3}). While the difference in improvement of one simulation over the other is small, both simulations demonstrate the same systematic shift seen in the Palestine simulations, where wilting point acts as a limiting lower bound. Knowing this, the accuracy of each simulation's SD to measured data SD is worth noting.

The 1-RAE and NSE indices were negative for both simulations which indicate poor prediction of θ regarding overall trends; however, this is expected because of the restriction of the wilting point as the lower bound of plant available water. The look-up table value of wilting point is preventing the simulations from accurately modeling measured θ. Although week 37 and 39 wetting periods showed the simulations wet the soil quicker than measured, the subsequent dry downs were well simulated. While the heterogeneity simulation produced slightly more accurate statistics than the homogeneity simulations, the improvement is very small. The results are similar for the next sandy loam layer.

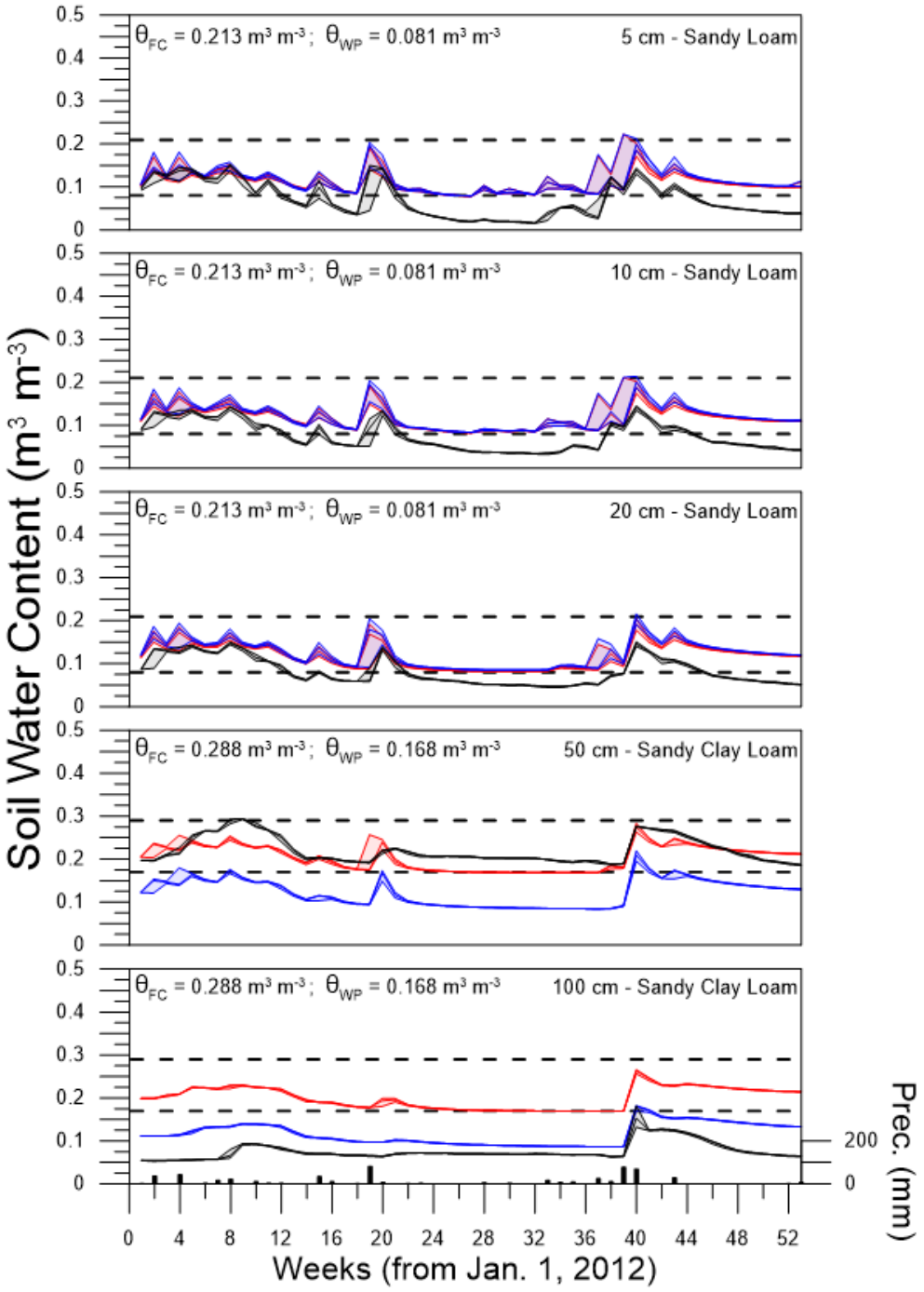

Figure 4. Modeled versus measured weekly soil water contents for a profile of Miles fine sandy loam in Bronte, TX. Weekly water contents indicate the interquartile ranges and medians for measured (black), simulated homogeneous (blue), and simulated heterogeneous (red) soil profiles at five depths. Weekly precipitation totals are on the x-axis.

The argillic horizon occurs at 50 cm depth where the texture changes to a sandy clay loam. The most apparent difference at this simulated depth is the systematic bias in the homogeneous simulation which predicted low θ. The heterogeneous simulation maintained a $\bar{\theta}$ (0.21 m^3 m^{-3}) similar to measured (0.22 m^3 m^{-3}). Also, the SD of the heterogeneous simulation was very similar to measured ($|\Delta SD|$ = 0.0003 m^3 m^{-3}). Further, the heterogeneous simulation (MAE and RSME) were ~25% of the homogeneous simulation errors. The high D values of both simulations indicate that the trends of both simulations were excellent, but heterogeneous modeled the measured trend more precisely than homogeneous. Clearly, the statistics and time series depict the superior θ predictions of heterogeneous, which included the argillic horizon.

In contrast to the 50 cm depth, the 100 cm depth with a sandy clay loam texture was simulated best by the homogeneous texture. The heterogeneous and homogeneous simulations overestimated θ, on average, by 0.12 and 0.04 m^3 m^{-3}, respectively. The heterogeneous simulation overestimated θ because the initialization of a clayey texture set the permanent wilting point and field capacity values higher than the apparent values of measured θ, which are more like a sandy loam (Table 4). The SD, RAE, and NSE values were both quite negative for both heterogeneous and homogeneous simulations, likely because both scenarios were only offset (Figure 4). The heterogeneous and homogeneous simulation D-indices were 0.87 and 0.95, respectively. The failure of both simulations to adequately simulate θ beyond matching trend raises suspicion of the measured θ values at 100 cm. According to a database of over 850 sandy clay loams in Texas, the average

Table 7. Statistical summary of heterogeneous and homogeneous-simulation results for soil water content at Bronte, TX.

Soil Water Content Source	Profile Depth	$\bar{\theta}$	SD	$\lvert\Delta SD\rvert$	Bias	MAE	RMSE	1-RAE	NSE	D
	cm	---------- $cm^3\ cm^{-3}$ ----------								
Measured Heterogeneous Profile	5	0.073	0.042	-	-	-	-	-	-	-
	10	0.076	0.034	-	-	-	-	-	-	-
	20	0.083	0.033	-	-	-	-	-	-	-
	50	0.22	0.031	-	-	-	-	-	-	-
	100	0.077	0.022	-	-	-	-	-	-	-
Heterogeneous Profile	5	0.12	0.037	0.0045	**0.044**	**0.045**	**0.054**	**-0.23**	**-0.67**	**0.93**
	10	0.12	0.037	**0.0024**	**0.046**	**0.046**	**0.054**	**-0.53**	**-1.5**	**0.94**
	20	0.12	0.036	**0.0032**	**0.038**	**0.038**	**0.045**	**-0.34**	**-0.9**	**0.95**
	50	0.21	0.031	**0.0003**	**-0.016**	**0.025**	**0.028**	**0.05**	**0.14**	**0.97**
	100	0.2	0.025	0.0032	0.12	0.12	0.12	-7	-31	0.87
Homogeneous Profile	5	0.12	0.039	**0.0025**	0.047	0.047	0.056	-0.29	-0.79	0.93
	10	0.13	0.039	0.0045	0.049	0.049	0.056	-0.63	-1.7	0.93
	20	0.13	0.038	0.0051	0.044	0.044	0.05	-0.54	-1.3	0.94
	50	0.12	0.034	0.0036	-0.097	0.097	0.1	-2.7	-9.6	0.9
	100	0.12	0.025	**0.0032**	**0.039**	**0.040**	**0.044**	**-1.6**	**-3**	**0.95**

† $\bar{\theta}$ is annual mean soil water content; $\lvert\Delta SD\rvert$ is the absolute difference between measured and simulated SD; MAE is mean absolute error; RAE is relative absolute error; and D is Willmott's index of agreement.

‡ Bold numbers indicate better overall simulation of measured data.

wilting point and field capacities are 0.16 and 0.29 m^3 m^{-3}, respectively (Kishne et al., 2017). In the measurements, the minimum values were 0.06 and 0.13 m^3 m^{-3}, respectively which better represents the reported range measured at 100 cm. However, this sandy clay loam layer at Bronte has 30 % clay, which is on the upper end of clay content in a sandy clay loam texture class. Therefore, this soil is expected to have near or above the average soil moisture values for the sandy clay loam texture class. However, the measured θ values appear to be too low for the documented texture and the evidence from simulations suggests the sensor may not be installed or calibrated properly at this depth. From the results of simulating the Bronte soil, a couple of summary observations can be made about the estimated θ. First, as in Palestine, homogeneous and heterogeneous soil simulation of θ were similar to each other for the sandier textures at the soil surface. Second, the heterogeneous simulation of the textural change at 50 cm matched the measured θ.

To summarize the statistical results of simulated water content for both sites, the homogeneous simulation did not account for the change in texture with depth nor the presence of an argillic horizon. The presence of an argillic horizon increased plant available water and changed the values of permanent wilting point and field capacity. The heterogeneous soil texture simulation was able to account for this effect of the argillic. If a soil profile has textures that are significantly different between the surface and subsurface and a constant wilting point is simulated for the entire profile, a poor estimation of θ should be expected at depths with very different wilting points compared to the soil surface.

Surface Heat Flux Partitioning

While soil θ is important to estimate for redistribution and plant uptake, the partitioning between latent and sensible heat from land surface models, because of soil θ, is needed for atmospheric models. Latent heat flux is an energy exchange that depends on soil θ through evapotranspiration; whereas, sensible heat flux is an energy exchange that is driven by vegetation surface temperature. Surface energy is partitioned between latent and sensible heat and can change based on heterogeneous and homogeneous soil profile simulations.

Figures 5 and 6 show the differences between heterogeneous and homogeneous soil profile simulations of the daily average of daytime latent (Δlatent) and sensible (Δsensible) heat fluxes for the summer of 2012 (1 June to 1 October) for Palestine and Bronte conditions. The Δstorage represents the difference in daily soil profile water storage between heterogeneous and homogeneous soil profile simulations. When Δlatent or Δsensible is positive, the respective heat fluxes from the heterogeneous simulation are greater than the heat fluxes from the homogeneous simulation. For example, when Δlatent is negative and Δsensible is positive, then the homogeneous simulation is partitioning more latent heat flux than the heterogeneous simulation. In contrast, when the Δlatent is positive and Δsensible is negative, then the heterogeneous simulation is partitioning more latent heat flux than the homogeneous simulation. Finally, when both Δlatent and Δsensible are positive, then the homogenous simulation is partitioning more energy to soil

storage, which raises soil temperature. Soil temperature rises in the homogenous simulation because the sandy soil holds less water.

Palestine, TX

In Palestine, the heterogeneous simulation had at least 16 cm more water storage than the homogeneous simulation (Fig. 5). The Δstorage started out at about 17.5 cm and increased rapidly to 19.5 cm over 10 days. During this soil-water recharge period, the Δlatent decreased from 1.5 to -86 W m^{-2}, while Δsensible increased from 2.2 to 22.8 W m^{-2}. This means the homogenous simulation is partitioning much more energy to latent heat than the heterogeneous. The homogeneous simulation generated more evapotranspiration during this wetting period because the sandier soil held less rainwater

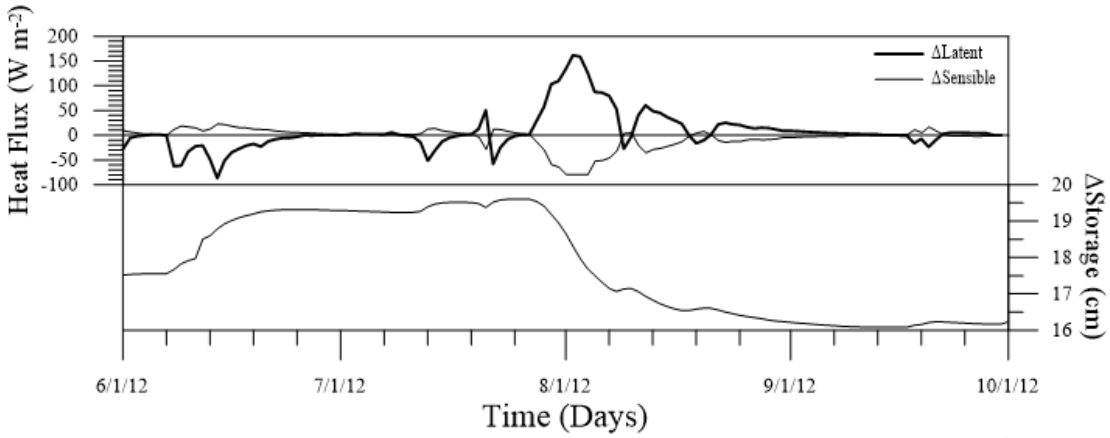

Figure 5. Profile water storage (Δstorage; cm), latent heat flux (Δlatent; W m^{-2}), and sensible heat flux (Δsensible; W m^{-2}) differences between heterogeneous and homogeneous soil simulations (e.g. Heterogeneous - Homogeneous) each day from June 1st through October 1st in Palestine, Texas. Hourly daytime changes in latent and sensible heat are plotted as a daily average, while water storage differences are plotted for each day.

in the whole profile versus the simulation of heterogeneity. This, in turn, forced the calculation of higher vegetation stress in the homogeneous simulation prior to the rain events. The Δlatent returns to a difference of 0 W m^{-2} as the stress index of the homogeneous simulation.

Following the relative stability from mid-June to about July 27th, the Δstorage reduces by about 2.5 cm of water over a 15-day dry-down period causing vegetation stress. As Δstorage decreased, Δlatent increased (-1.5 to 161.8 W m^{-2}), and then decreased (to 53.2 W m^{-2}). The change in Δsensible reflected this trend. The changes during this period mean: 1) the simulation of heterogeneity partitioned more latent heat flux and less sensible heat flux than the homogenous simulation, 2) lower latent heat generated from the homogeneous simulation was a result of more vegetation stress, and 3) the increased stress was due to the vertically homogeneous loamy sand storing less water than an argillic horizon would provide. The decrease of Δlatent from the maximum value is simply the heterogeneity simulation's vegetation eventually succumbing to water stress caused during this dry-down. This overall pattern is common during the latter half of the summer.

Several points can be made from these results. First, Δstorage indicated that more water was stored in the heterogeneous profile than the homogeneous profile. Clearly, a soil with sandy clay loam texture will store more water than a sandier soil (Table 2). Second, increases in Δstorage coincided with increased latent heat flux and decreased sensible heat flux of the homogeneous simulations due to evaporation. Thirdly, decreases in Δstorage coincided with increased latent heat and decreased sensible heat of the heterogeneous simulations due to increased water storage. This period was evidence of

vegetation stress in the homogeneous simulation caused by the low soil water storage and lack of significant rainfall for over a month. The take home observation from Fig. 5 is that accounting for vertical soil heterogeneity in Palestine, located in an udic soil moisture regime, reduced surface evaporation, increased water storage, and reduced vegetation stress, all of which contributed to further partitioning of latent heat.

Bronte, TX

In Bronte, the heterogeneous simulation had at least 15 cm more summer water storage in the soil profile than the homogeneous simulation (Fig. 6). The excess 15 cm of water represents the soil water storage added by accounting for sandy clay loam in the heterogeneous simulation. The Δstorage decreased by only 0.25 cm over 40 days, but this is expected due to low precipitation and an ustic soil moisture regime. Figure 6 shows a 40-day period of soil drying with no precipitation. During this time, Δlatent decreased from around 10 to 0 W m^{-2}, whereas Δsensible increased from about -10 to -1 W m^{-2}, on average. The decreasing Δlatent and increasing Δsensible indicates that the heterogeneous scenario started with more evapotranspiration because there was more water stored in the clayey layers. Over the 2.5 months of dry conditions, Δlatent hovered around 0 or -1 W m^{-2} and Δsensible hovered between 0 and -2 W m^{-2}. The fact that both Δlatent and Δsensible were negative is indicative of increased soil heat flux in the heterogeneous soil due to increased water content.

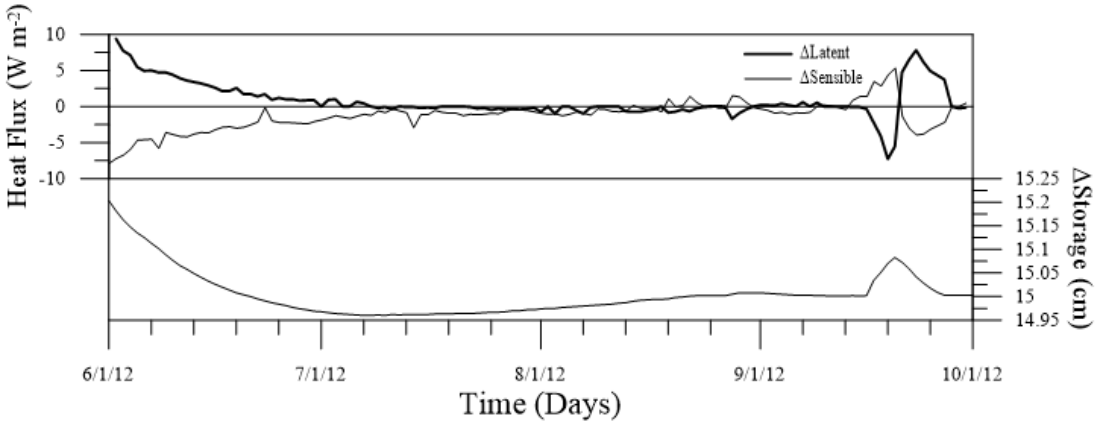

Figure 6. Profile water storage (Δstorage; cm), latent heat flux (Δlatent; W m^{-2}), and sensible heat flux (Δsensible; W m^{-2}) differences between heterogeneous and homogeneous soil simulations (e.g. Heterogeneous - Homogeneous) each day from June 1st through October 1st in Bronte, Texas. Hourly daytime changes in latent and sensible heat are plotted as a daily average, while water storage differences are plotted for each day.

After September 15th, the Δstorage briefly increased by 1 mm caused by a rainfall event. During the change in Δstorage, the Δlatent decreased to -7.5 W m^{-2} and followed by a peak near 8 W m^{-2} just after the 18th. In contrast, Δsensible increased to 5 W m^{-2} by the 18th followed by a minimum of -4.5 W m^{-2}, afterwards. The initial large decrease in Δlatent and increase in Δsensible indicates when the homogeneous scenario's vegetation began to heavily transpire, relative to the heterogeneous scenario's vegetation. The abrupt switch to a positive Δlatent and negative Δsensible indicates that the heterogeneous scenario's vegetation was able to transpire for a longer time due to the high soil water storage capacity of the sandy clay loam and the decreased geometric mean of hydraulic conductivity in the heterogeneous profile.

From these results, some observations become apparent. First, the Δstorage showed the increase in total water storage by the sandy clay loam texture in the subsoil of

the heterogeneous simulation. Second, the heterogeneous scenario partitioned more latent heat flux than the homogeneous scenario during dry downs. The increased partitioning of latent heat flux demonstrated the effect of texture on available water storage for evapotranspiration. Given the differences in simulated energy from both sites, textural heterogeneity of an abrupt argillic did affect simulated heat flux outputs through the increase in available water that could be stored and later transpired.

Linear Regressions of Both Sites

As another approach to confirm the effects of soil heterogeneity on surface heat, partitioning is plotted as latent heat fluxes versus their sensible heat flux counterparts (Fig. 7). The slopes of the regression curves represent the partitioning of the heat fluxes, where higher slopes indicate an increase in latent heat partitioning versus sensible heat partitioning. Red dots, lines, and shading represent the hourly daytime heat flux values, regression slopes (m), and 95% confidence intervals from the summer of the heterogeneous simulation, whereas blue represents heat flux values, regression slopes, and 95% confidence intervals from the summer of the homogeneous simulation.

As shown in Fig. 7, the regression slope for the heterogeneity simulation of Palestine ($m_{Hetero} = 0.13$) depicts significantly ($\alpha = 0.05$) increased latent heat partitioning compared to the texturally uniform and sandy homogeneous simulation's slope ($m_{Homo} = -0.06$). The slopes of Bronte simulations were not significantly ($\alpha = 0.05$) different from

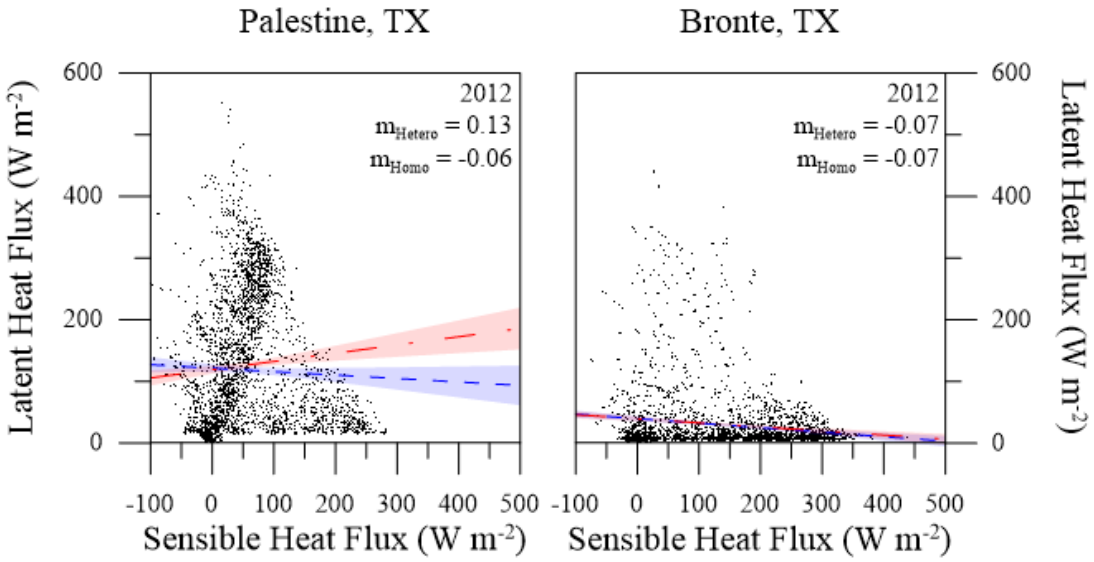

Figure 7. Linear regressions and 95% confidence intervals of hourly latent versus sensible heat (W m^{-2}) for the months of June through September in 2012. Red and blue colors represent vertically heterogeneous and homogeneous soil profile textures, respectively. The regression slopes are represented as m_{Hetero} or m_{Homo} for the heterogeneous and homogeneous simulations, respectively.

each other, which indicates that heat flux partitioning between simulations were relatively similar. Palestine receives increased precipitation versus Bronte; so, the effect of increased simulated water storage from the argillic layers on heat flux partitioning is more apparent for Palestine, which is a more humid environment.

The linear regressions and the surface heat flux differences between heterogeneity and homogeneity simulations highlight that modeling soil texture heterogeneously with depth does affect the partitioning of latent heat fluxes; so long as, the amount of precipitation and, subsequently, water storage is significant enough to affect evapotranspiration multiple times across the summer. For example, in 2012, Palestine received 35.6 cm of rainfall and Bronte received 22.2 cm during the summer months. In

addition to the heat flux analyses, soil water was modeled more accurately in the argillic, or claypan, when vertically heterogeneous soil textures were initialized for the entire simulated soil profile. Therefore, the accuracy of vertical soil representation directly improves the accuracy of soil water content and storage simulated by biophysical models. Furthermore, the accuracy of vertical soil representation indirectly affects surface heat flux outputs of biophysical models, particularly when simulating soils with moderate precipitation and udic soil moisture regimes relative to dry and ustic conditions, as detailed in the following sections.

Sensitivity of Heat Flux Partitioning to Claypan Depth

The results indicate that accurate modeling of soil texture along the soil profile is important to modeling the soil moisture. Because vertical heterogeneity of soil texture can significantly (α=0.05) affect surface heat flux partitioning, particularly in an udic soil moisture regime with adequate precipitation, it is of interest to evaluate the sensitivity of heat flux partitioning to the depth of claypan as well as the texture changes. For the second phase of this project, a partitioning analysis was performed prior to a sensitivity analysis. The partitioning analysis examined latent versus available heat flux partitioning, or evaporative fraction, and water balance partitioning to ascertain the sensitivity of latent heat to changes in claypan depths, strong textural dichotomies, and depth of root growth. The sensitivity analysis examined the detailed changes in latent heat flux as the claypan interface depths, soil textures, and rooting depths changed.

The simulated scenarios used for both analyses are defined by the following abbreviations:

A refers to the actual soil texture from the CRN sites;

SC refers to a strong change in texture class (e.g. sand over clay);

180 refers to a vegetation rooting depth of 180 cm; and

80 refers to a vegetation rooting depth of 80 cm.

For example, an A180 scenario of Palestine initializes RZWQM2 with soil profile textures from Palestine down to 200 cm deep using vegetation with a maximum rooting

depth of 180 cm. The A180, SC180, and SC80 scenarios were implemented in RZWQM2 as different initializations with weather data from 2011, 2012, and 2013.

The analysis of the results includes the four months of June 1 to Oct 1 from each year. The 30-year average rainfall for the months of June through September in Palestine TX is 35.9 cm. In comparison, 2011 was a very dry summer with 8.4 cm of precipitation; 2012 was average with 35.6 cm, and 2013 was slightly drier than average at 29.2 cm. At Bronte, the 30-year average is 21.5 cm. Again, 2011 was very dry with 2.7 cm of precipitation; 2012 was average at 22.2. cm; and 2013 was relatively wetter than average with 29.2 cm.

Partitioning Analysis

The simulated heat flux partitions are visualized as average monthly evaporative fractions (Fig. 8 and 10) and summer water balance partitions are represented as a collection of bar charts (Fig. 10 and 12). The average monthly evaporative fractions and summer water balances are depicted as sub-figures in a grid pattern where A180, SC180 and SC80 are in columns and the years of 2011, 2012, and 2013 are in rows (Fig. 8-11). Each sub-figure within the grids are referred to by year and initialization (e.g. 2012-SC180). The sub-figures depict three RZWQM2 simulations with 5, 20, and 100 cm claypans.

Palestine, TX

Palestine, TX has a temperate climate with moderate precipitation, which creates pattern of evaporative fraction, seen in Figure 8. The average monthly evaporative fraction decreases during the winter months and has a dip in evaporative fraction around July and August during the stress of midsummer. In the claypan depth simulations using actual soil texture, there is no effect of clay pan depth in evaporative fraction. In Figure 8, there are two seasonal patterns of evaporative fraction that recur for all simulations and depict the differences in wintertime and summertime evaporative fractions between the simulated claypans. During the winter, evaporative fractions increase for deeper claypans; whereas, in summer evaporative fractions increase for shallower claypans.

The differences between the simulated evaporative fractions during the winter months are largely apparent after the soil texture is changed in SC180. Average winter month evaporative fractions tend to be below 0.5 because transpiration was negligible. The only significant contribution to latent heat during the winter months was through evaporation. As a result, soils that were simulated with a higher water storage, a lower hydraulic conductivity, and a shallow claypan produced more drainage than evaporation. Soils with increased drainage had less latent heat than soils that produced more evaporation.

There are small evaporative fraction differences between the 3 heterogeneous claypan simulations (A180) for Palestine and Bronte. The overall summer trend is that evaporative fraction increases for deeper claypans. Deeper claypans have more profile

PAW than shallower claypans because they have more sandy loam soil (Tables 4 and 8). The gains in profile PAW decrease as the sandy loam replaced sandy clay loam in deeper

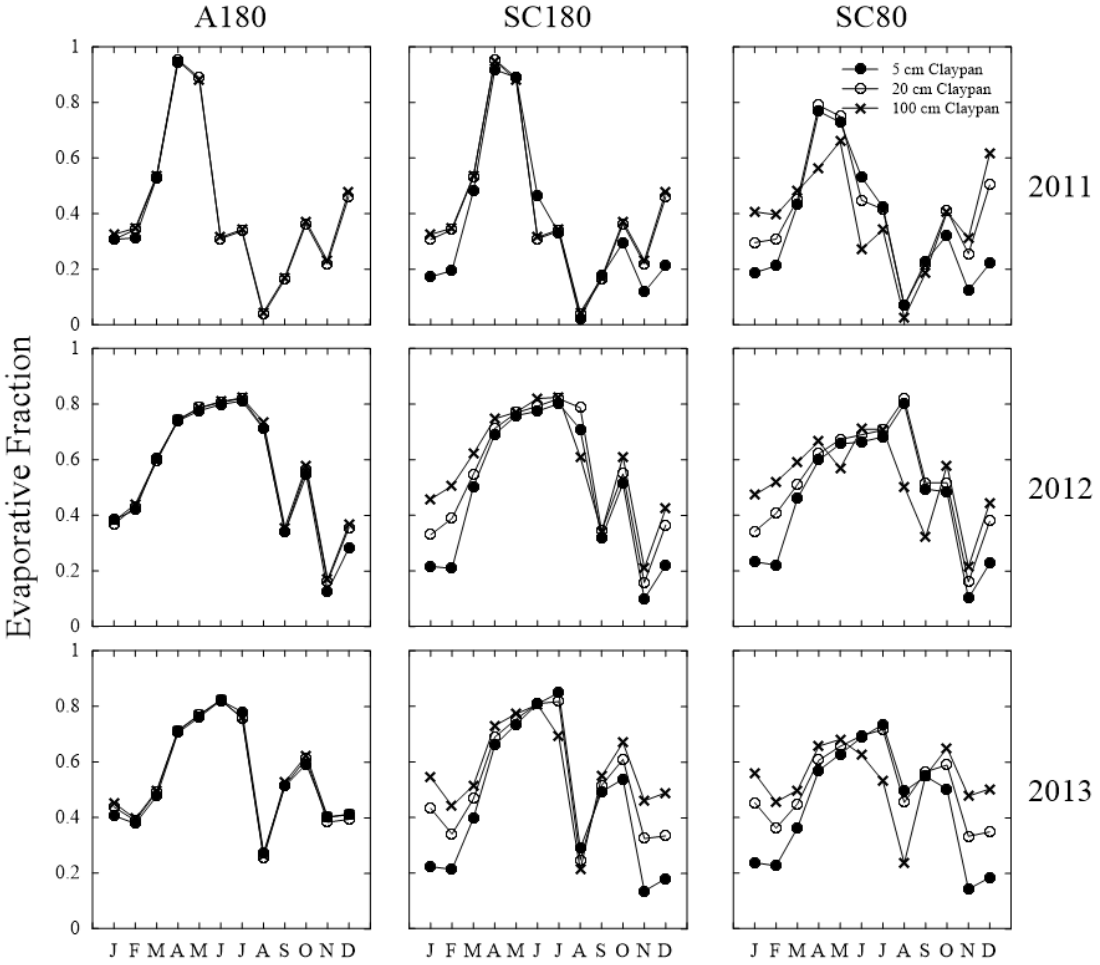

Figure 8. Evaporative fractions for Palestine, TX, averaged monthly, represent the daytime hourly latent heat flux partitioning of the available surface heat fluxes (latent+sensible) generated by RZWQM2. The filled circles, empty circles, and crosses represent the simulation of 5, 20, and 100 cm deep claypan interfaces, respectively. The A180 column of charted simulations are initialized with measured soil textures and 180 cm rooting depth. The SC180 column of charted simulations are initialized with sand and clay textures and a 180 cm rooting depth. The SC80 column of charted simulations are initialized with sand and clay textures and an 80 cm rooting depth.

Table 8. Plant available water and profile water storage examples of Palestine simulations. Demonstrates decreasing gains by deepening the claypan of site textures and increasing losses for sand over clay textures.

Claypan Depth	Palestine Textures		Sand over Clay	
	PAW	Storage	PAW	Storage
	---------- cm ----------			
5	21.4	74.8	25.3	100.7
20	21.4	74.7	24.1	99.1
100	22.3	74.4	17.6	90.8

claypan simulations. In the case of the sand over clay (SC180 and SC80), losses in PAW increase as the claypan deepens.

The increased summertime differences between the three simulated claypan depths were exaggerated by changing the soil texture in SC180 and further exaggerated by simulating shallow rooting vegetation in SC80. The increases to the latent heat partitioning within the evaporative fractions of shallow claypans were primarily due to the increased soil water storage and PAW of shallow clays within the root zone of simulated vegetation. As expected, total available water decreased as claypans were simulated deeper within the profile and as roots were shortened (Fig. 9), except in 2011-SC80.

The drought during 2011 did not produce enough precipitation to affect the differences in evaporative fraction between 2011-SC180 claypan simulations during most of the summer months. By shortening the maximum rooting depth to 80 cm, the

evaporative demand of vegetation was reduced, which extended the duration of transpiration during the 2011-SC80 summer months. The extended transpiration only increased transpiration during periods of low precipitation, such as in 2011. The need for deep soil moisture for transpiration illustrated the effect of claypan depth and soil texture

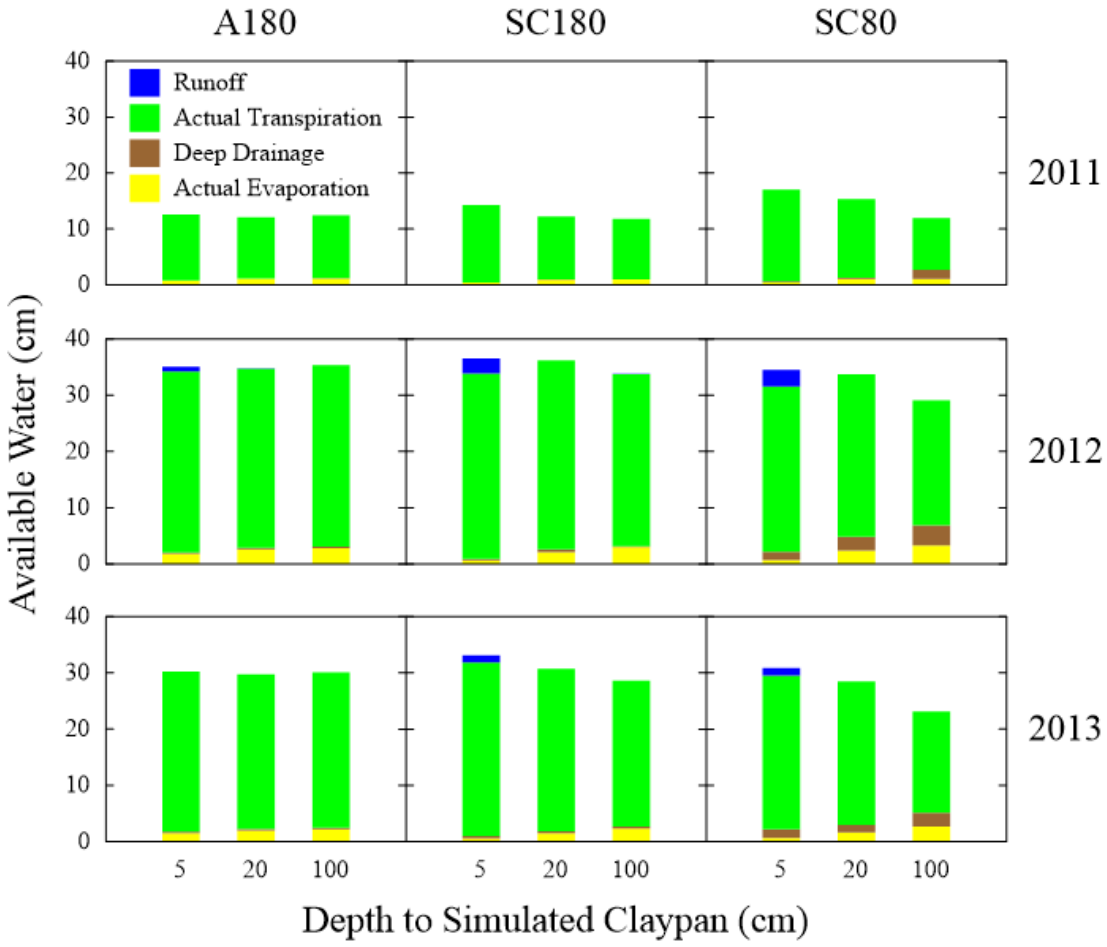

Figure 9. Water balance results for Palestine, TX for June through September of 2011, 2012 and 2013. Simulations with different depths of the claypan are depicted on the x-axis. Water available to partition (cm) is the total soil column water minus precipitation. The A180 simulations are initialized with measured soil textures and 180 cm rooting depth. SC180 simulations are initialized with sand and clay soil textures and a 180 cm rooting depth. SC80 simulations are initialized with sand and clay soil textures and an 80 cm rooting depth.

on average monthly evaporative fractions during some summer months in 2011, 2012, and 2013.

Overall, evaporative fraction increased for deeper claypans during the winter months and for shallow claypans during summer months. Interestingly, the average monthly evaporative fraction for the 5 cm claypan in August 2012 was less than the deeper 20 cm claypan in both the SC180 (~0.1) and SC80 (~0.025) simulations. The decreased evaporative fractions of the 5 cm claypan simulations were a result of more runoff (~3 cm; Fig. 9), induced by the shallow claypan. The lower evaporative fractions of the 5 cm claypan simulation demonstrates how lower infiltration capacity of a shallow claypan can decrease the evaporative fraction by preventing water from infiltrating into the soil.

Bronte, TX

Bronte, TX is in a drier climate than Palestine. Figure 10 shows patterns of evaporative fraction for a much drier climate. Again, the winter months generated the larger difference in evaporative fraction between the claypan depth simulations, if a difference existed. In the contrasting soils, deeper claypans had larger evaporative fractions. Deeper claypans also had larger evaporative fractions in the summer months in the contrasting texture claypans. The differences were dampened by the drier climate and ustic soil moisture regime. Except for April 2011, June 2012, and April 2013, the simulation of Bronte's environment did not provide enough water to determine if soil texture could significantly affect latent heat partitioning.

To add water to the simulation without directly increasing precipitation, or altering the soil initialization, or calibrating the model, the maximum rooting depth was made shallow. In other words, shallow root depth in SC80 lowered the transpiration rate,

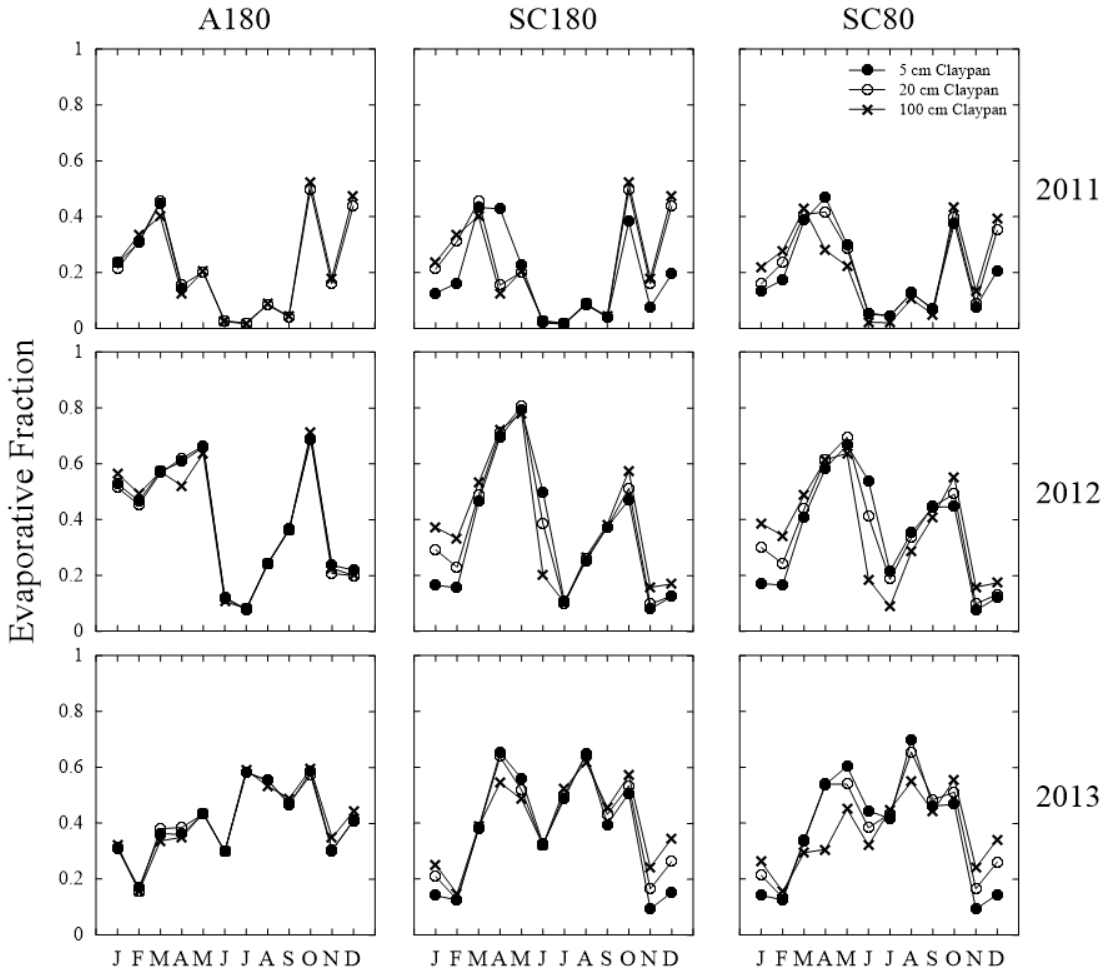

Figure 10. Evaporative fractions at Bronte, TX, averaged monthly, represent the daytime hourly latent heat flux partitioning of the available surface heat fluxes (latent+sensible) generated by RZWQM2. Filled circles, empty circles, and crosses represent the simulation of 5, 20, and 100 cm deep claypan interfaces, respectively. The A180 column of charted simulations are initialized with measured soil textures and 180 cm rooting depth. The SC180 column of charted simulations are initialized with sand and clay textures and a 180 cm rooting depth. The SC80 column of charted simulations are initialized with sand and clay textures and an 80 cm rooting depth.

increased the duration of transpiration throughout each month, and increased the differences between the average monthly evaporative fractions of each SC80 claypan simulation. The SC80 simulations in Figure 11 depict an increased duration of summer transpiration during years with below average precipitation, 2011 and 2012. In an average

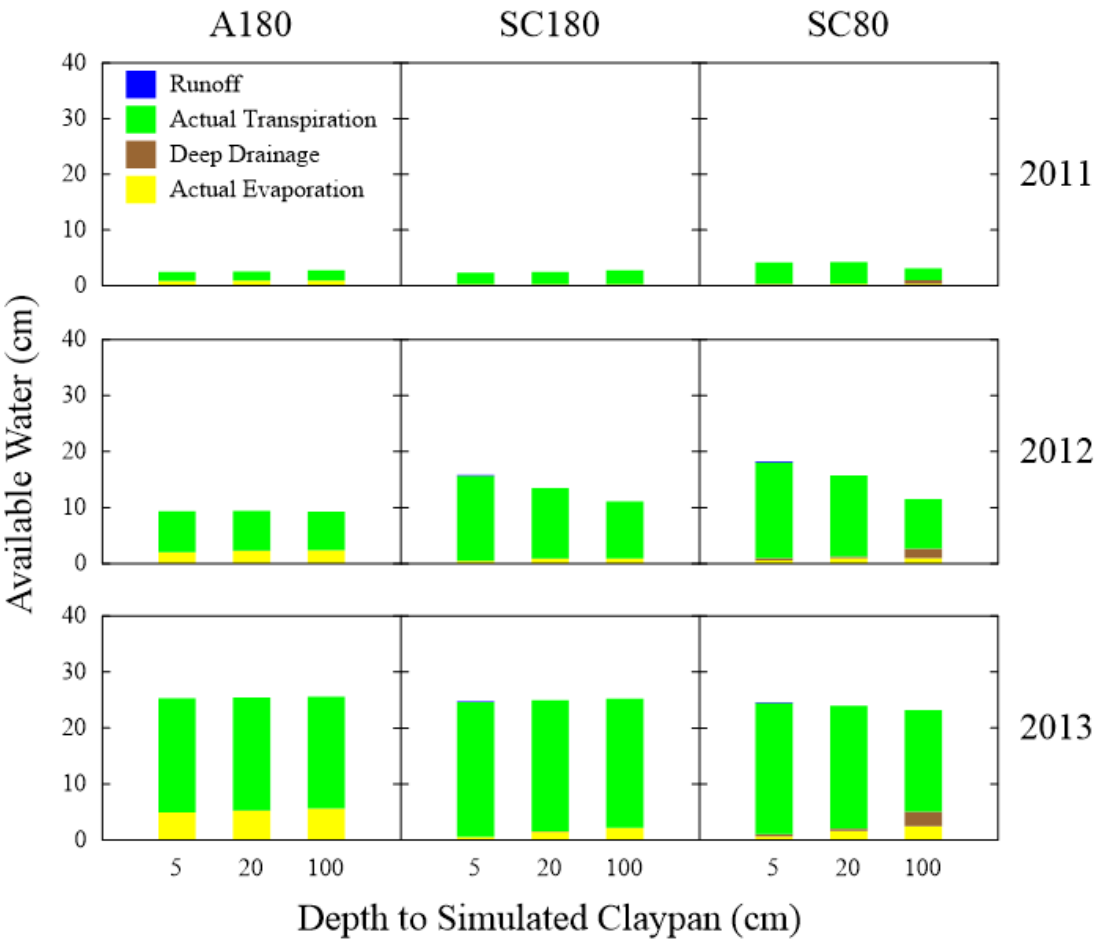

Figure 11. Water balance results for Bronte, TX for June through September of 2011, 2012 and 2013. Simulations with different depths of the claypan are on the x-axis. Water available to partition (cm) is the total soil column water minus precipitation. The A180 simulations are initialized with measured soil textures from Palestine and 180 cm rooting depth. The SC180 simulations are initialized with sand and clay soil textures and 180 cm rooting depth. The SC80 simulations are initialized with sand and clay soil textures and an 80 cm rooting depth.

precipitation year, 2013, had a decrease in transpiration. The magnitude of differences in evaporative fraction for SC80 was caused by the reduced evaporative demand of the shallow roots. The differences in evaporative fraction between claypan depths were a result of the contrast between the two claypan textures and depth of the simulated claypans. By decreasing the maximum rooting depth in SC80, the average monthly evaporative fraction of the 100 cm claypans stand apart from the shallower claypan evaporative fractions because the vegetation could not uptake PAW in the deep clays. Furthermore, the evaporative fractions of the 5 cm claypan simulations have noticeably increased, versus their 20 cm claypan counterparts, due to the increased soil water storage of shallow clays within the root zone.

To summarize, the soil texture and claypan depth of a soil are affecting the partitioning of latent heat as seen in the evaporative fractions of all three claypan simulations for both sites. As the claypan simulations deepened in the soil profile, the summertime evaporative fractions decreased and the winter time evaporative fractions increased. However, the decreased contrast in texture coarseness between the surface and claypan for A180 simulations produced no significant differences in the evaporative fractions or water balances between the three claypan simulations. Therefore, an udic or ustic claypan soil with a large contrast in texture about a claypan can increase or decrease the partitioning of latent heat fluxes based on the season, precipitation, vegetation growth, and the depth to the claypan's interface.

Sensitivity Analysis of Latent Heat Fluxes to Claypan Depth

While the partitioning analysis revealed how latent heat fluxes are affected by an increase in textural contrast about the claypan, the sensitivity of latent heat fluxes to the depth of a claypan is not understood as well as seasonal, precipitation, and vegetative growth effects. In the previous section, the partitioning analysis resulted in the following observations: 1) The A180 simulations of the 5, 20, and 100 cm claypan depths partitioned latent heat similarly because the surface and subsurface textures lacked a significant contrast in coarseness; 2) the SC180 initialization amplified the differences in latent heat partitioning between each simulation by increasing the textural contrast of coarseness at the claypan interfaces of A180 simulations; and 3) the SC80 initialization amplified the simulated differences in latent heat partitioning between each simulation for claypans under droughty climates by limiting root depth compared to SC180 simulations. Overall, the effect of texture was apparent and modified the heat from evapotranspiration by increasing or decreasing profile water storage and heat storage. This successfully altered the partitioning of available water and latent heat, while providing initial evidence that various claypan depths alter the surface heat flux. However, the sensitivity of the changes to water balancing and latent heat as a claypan deepens are not fully understood and will now be explored.

As the initializations were changed from A180 to SC180 to SC80, the water balance partitions (runoff, deep drainage, actual transpiration, or actual evaporation) increased or decreased between the 5, 20, and 100 cm claypan depth simulations. Figures

13 and 15 depict how the water is partitioned differently between the three simulations (A180, SC180, and SC80). For simulations from A180 to SC180 to SC80, the changes in textural contrast and root depth changed water available for partitioning and the result is summed so that SC180-A180 depicts change in textural contrast, and SC80-SC180 depicts change in root depth (Figs. 13 and 15). Since only the evapotranspiration terms directly relate to the latent heat fluxes, the subsequent analysis focuses closely on evaporation and transpiration. The runoff and deep drainage were used to clarify where losses in latent heat partitioning occurred.

Figures 12 and 14 show how the differences in water partitioning altered the range of latent heat partitioning for potentially deeper or shallower claypan depths at Palestine (udic) and Bronte (ustic). In Figures 12 and 14, the interquartile ranges of log-adjusted latent heat fluxes (W m^{-2}) were plotted versus an increasing claypan interface depth (cm), which are defined in this thesis as heat flux profiles. Each heat flux profile within the figures are referred to by year and then initialization (e.g. 2012-SC180). Each heat flux profile represents a set of simulations representing 10 cm increases in depth-to-claypan-interface from 0 cm (homogeneous clay) to 200 cm (homogeneous sand). The completely clay homogenous simulation (0 cm) is not included for SC180 conditions in 2013 due to instability in the water balance solution. The heat flux profiles depict how latent heat partitioning changes with claypan interface depth. When latent heat values are small, small interquartile ranges indicate significant plant stress, and wide interquartile ranges indicate some plant stress. When latent heat values are large, wide interquartile ranges indicate little plant stress, and short interquartile ranges indicate no plant stress.

Palestine, TX

As previously mentioned, Palestine experienced the most precipitation in 2012, less in 2013, and extreme drought in 2011. The heat flux profiles (Fig.12) reflected the differences in precipitation between each year, where the 2012-A180 interquartile range had the highest latent heat flux values with a wide range (high transpiration, high soil water content, low plant stress), the 2013-A180 interquartile range had lower het flux values and a shorter range (lower transpiration, lower soil water content, higher plant stress) , and the 2011-A180 interquartile range had the smallest heat flux values and the shortest range (lowest transpiration, lowest soil water content, highest plant stress). The heat flux profiles also reflect the partitioning of latent heat from the evaporative fractions (Fig. 8) and partitioning of evaporation and transpiration in the bar charts (Fig. 9). The evidence of increased latent heat flux partitioning in 2012 as compared to drier years supports the sensitivity analysis methods of evaluating the heat flux profiles. Because of this, Figure 13 can be used while interpreting Figure 12.

The increased differentiation in texture change in SC180 (compared to A180) was previously shown to affect soil water storage by decreasing available water, resulting in decreases in latent heat fluxes (Fig. 3, 5 and 7). Referencing the average (wettest) year (2012), the heat flux profile in 2012-SC180 (compared to 2012-A180) depicted an interquartile range with a lower 25^{th} percentile (11 W m^{-2}) and a median that gradually decreased for deeper claypans (70 W m^{-2}) down to the maximum rooting depth. After the maximum rooting depth, the 25^{th} percentile and median increase down to a 200 cm

claypan. These profiles provide evidence that vegetation stress increases for a stronger difference in textural coarseness about the claypan interface, which was decreased for shallow claypans (≤ 20cm) and increased for deeper claypans (> 20 cm). Vegetation stress improved once the claypans were below the maximum rooting depth (Fig. 12). The

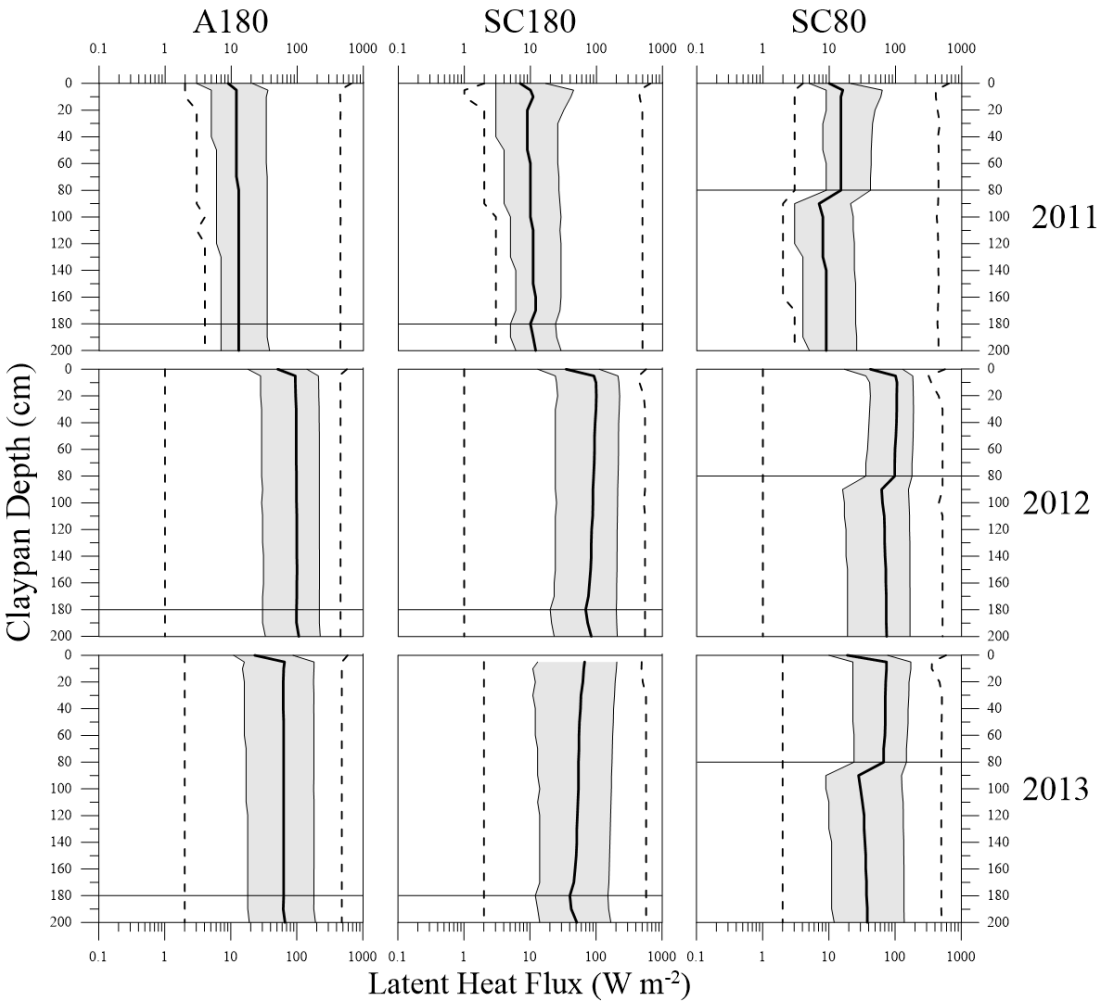

Figure 12. Heat flux profiles depicting the log-adjusted range of latent heat fluxes with increasing claypan depth for summers of 2011, 2012, and 2013 in Palestine, TX. The bold lines represent the median, shaded regions represent the interquartile range, and dashed lines represent the minimum and maximum of latent heat fluxes. The horizontal line in each graph depicts the rooting depth. A180, SC180 and SC80 are actual and sand over clay (SC) texture classes and 180 and 80 are rooting depths.

differences in evapotranspiration partitioning corroborate the differences in the heat flux profiles (2012; Fig. 13). When the claypan is shallow (5 cm) and the surface is sandy, runoff increases by 2 cm (cyan) as 1 cm of evaporation (yellow) becomes transpiration (lime). As the claypans are simulated deeper in the profile, transpiration increases (2 cm) with decreasing runoff (0.5 cm; ≤ 20 cm) and decreases (2 cm) for deeper claypans (> 20 cm) as their water storages of the soil profile decrease. For 2013, which was drier than 2012, the differences in water balance were similar, with runoff being a factor affecting water available for transpiration and with soil texture decreasing available water storage. The decreased precipitation in 2013 is reflected in the 2013-SC180 heat flux profile as a

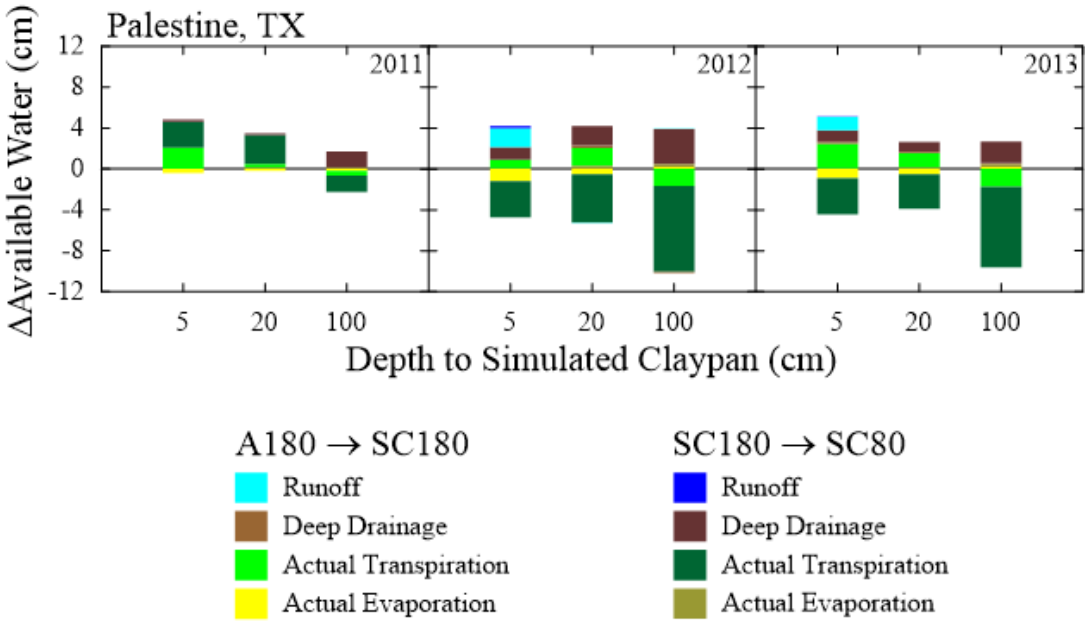

Figure 13. Water balance results depicting the effects of adjusted soil texture (A180 to SC180) and rooting depth (SC180 to SC80) across the summers of 2011, 2012 and 2013 for 5, 20, and 100 cm deep claypan depths. Simulations use weather data from Palestine, TX. Bright colors indicate changes from actual to extreme soil textures and muted colors indicate changes associated with shallower rooting depth.

left shift with decreased latent heat fluxes of a wider interquartile range demonstrating increased vegetation stress. The pattern of 2013-SC180 is like 2013-A180 when each profile is compared to their 2012 counterparts. The heat flux profile in 2011-SC180 had a wider interquartile range of decreased latent heat fluxes for shallow claypans, relative to 2012-SC180, that narrows rapidly toward the rooting depth. The decreasing interquartile ranges in the 2011-SC180 heat flux profile are further evidence of increasing vegetation stress as the claypan interface depth was lowered (Fig. 12). The relaxed vegetation stress of shallow claypans in 2011-SC180 is explained by the increased transpiration caused by the high storage capacity of the near-surface clay and absent runoff from the decreased precipitation of 2011.

The SC80 initialization for Palestine had the same precipitation and soil textures as SC180, but the root growth was shallow (80 cm). There are two patterns that are immediately apparent for the SC80 heat flux profiles. First, the change in yearly precipitation produces an increasing shift in the interquartile range for more precipitation and a decreasing shift for less precipitation, as seen in both the A180 and SC180 initializations (Fig. 12). Second, the shallower roots caused decreased vegetation stress for claypans at and above the maximum rooting depth and increased vegetation stress for claypans below the maximum rooting depth (Fig. 12). The increase in vegetation stress for deeper heat flux profile claypans corresponds well with the significantly decreased evaporative fractions (Fig. 8), and the decreasing transpirations with increased drainages (Fig. 9). Furthermore, from Figure 13, the loss in transpiration (muted green) exaggerates as the claypans deepen causing reduced available water storage (Fig. 9) and increased

hydraulic conductivity (drainage; Fig. 13) due to sand replacing clay in the root zone (Tables 3, 4, and 8). The transpiration in 2012 and 2013 depicts losses for shallow claypans (Fig. 13) because of the reduced transpiration requirements of shallow rooting vegetation (Table 5) with increased precipitation.

All results from Palestine simulations showed that in an udic soil moisture regimes: 1) modeling with accurate texture properties produced significantly ($\alpha = 0.05$) different latent heat fluxes compared to homogeneous simulations (Fig. 7); 2) modeling soil profile textures heterogeneously with an abrupt contrast in coarseness will generate increased latent heat flux partitioning for shallow claypans (< 100 cm) and decreased latent heat flux partitioning for deep claypan interfaces (>100 cm) when provided enough precipitation (Fig. 8, 9, and 12); 3) modeling soil profile textures heterogeneously with an abrupt contrast in coarseness and shallower roots will generate decreased latent heat fluxes for more summer days with increased latent heat flux partitioning where roots reach the claypan and decreased latent heat flux partitioning when the claypan is below the maximum rooting depth.

Bronte, TX

The Bronte simulations received the most precipitation in 2013, average precipitation in 2012, and was droughty in 2011. The heat flux profiles reflected differences in precipitation between each year, where the 2013-A180 interquartile range

had the largest values with the widest ranges and the 2011-A180 interquartile range had the smallest values with the shortest ranges (Fig. 14).

The stronger textural contrast of the SC180 initialization has been shown to affect soil water storage and surface heat fluxes (Fig. 4, 6, and 7). Referencing the wettest year,

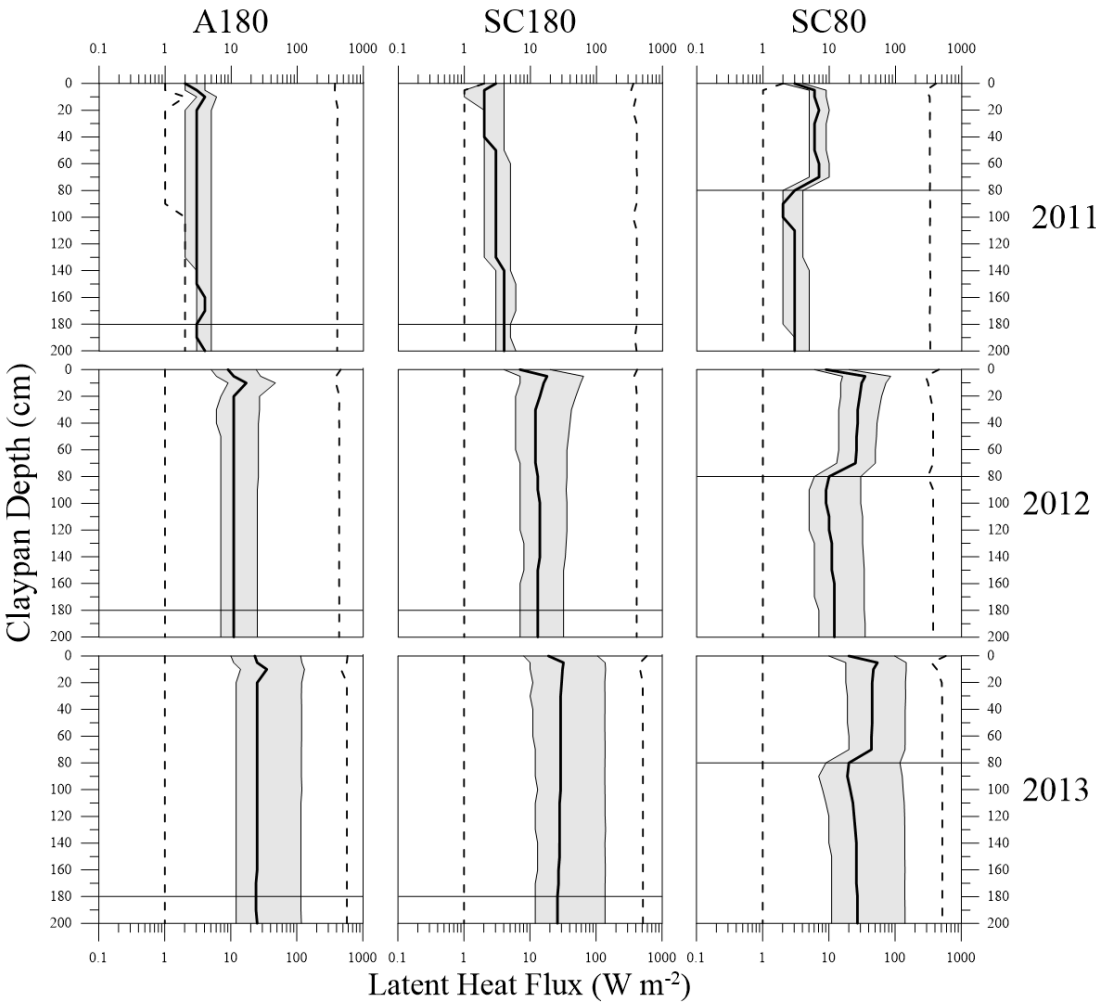

Figure 14. Heat flux profiles depicting the log-adjusted range of latent heat fluxes with increasing claypan depth for summers of 2011, 2012, and 2013 in Bronte, TX. The bold lines represent the median, shaded regions represent the interquartile range, and dashed lines represent the minimum and maximum of latent heat fluxes. The horizontal line in each graph depicts the rooting depth. A180, SC180 and SC80 are actual and sand over clay (SC) texture classes and 180 and 80 are rooting depths.

the heat flux profile in 2013-SC180 depicted an interquartile range that shifted negligibly from 2013-A180, but the interquartile range widened by approximately 22 W m^{-2}, which indicates reduced overall vegetation stress, relative to that observed in 2013-A180. This corresponds well with the reduced evaporative fractions (Fig. 10) and the conversion of evaporation (yellow) to transpiration (lime; Fig. 15). The overall decrease in evaporation in 2013-SC180 was due to the increased hydraulic conductivity of surface sand (K = 8.640 cm hr^{-1}; Table 4), which permitted rapid redistribution of soil water from the surface to the claypan, unlike the relatively slower conductivity of sandy loam (K = 3.636 cm hr^{-1}) in 2013-A180.

For the 2012-SC180 heat flux profile with average precipitation, the interquartile range is wider for shallow claypans and narrows for deeper claypans, relative to 2012-A180 claypans (Fig. 14). Additionally, the entire heat flux profile of 2012-SC180 maintained wider interquartile ranges without increasing or decreasing the shift, relative to the 2012-A180 claypans. As in 2013-SC180, this indicates less vegetation stress for the whole heat flux profile due to the change in soil texture (Fig. 15).

Drought conditions of 2011 created different patterns in the latent heat flux profiles heavily influenced by soil water storage and permanent wilting point. The shallow claypans of 2011-SC180 partitioned less latent heat flux than in 2011-A180, yet partitioned more latent heat flux for deeper claypans (Fig. 14). Meanwhile, transpiration increased 0.5 cm, replacing the surface evaporation (Fig. 15). This unusual circumstance is caused by the change in soil texture coarseness and their claypans' wilting points that were shallower than 150 cm. First, the change from a sandy loam texture to a sandy texture

increased the hydraulic conductivity, lowered the permanent wilting point, and lowered the available water storage. The sand was then capable of rapidly conducting water to deeper claypans without the extra requirement of a sandy loam wilting point removing water from availability. Second, the change from a sandy clay loam to a clay increased the wilting point and, consequently, the required water to maintain that water content as unavailable plant water storage. As both claypans in 2011-A180 and 2011-SC180 were decreased below 150 cm and replaced by coarser textures, the wilting point water storage requirement caused by the claypans' higher matric potential was removed enough to allow increased generation of transpiration from simulations in both initializations. This also

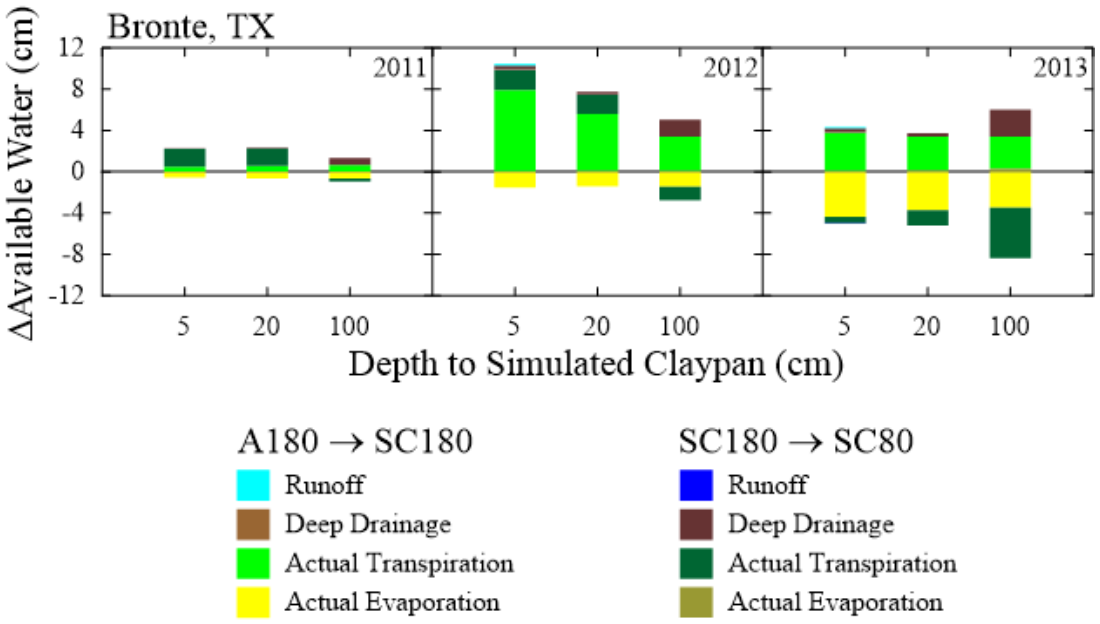

Figure 15. Water balance results depicting the effects of adjusted soil texture (A180 to SC180) and rooting depth (SC180 to SC80) across the summers of 2011, 2012 and 2013 for 5, 20, and 100 cm deep claypan depths. Simulations use weather data from Bronte, TX. Bright colors indicate changes from actual to extreme soil textures and muted colors indicate changes associated with shallower rooting depth.

explains the decreased latent heat fluxes of the shallow claypans of 2011-SC180 versus the increased latent heat fluxes caused by less abrupt textures of the 2011-A180 initialization at the same claypan depths.

The SC80 initialization for Bronte produced a consistent pattern in the affected latent heat flux profiles, just as the condition did in Palestine. The patterns all show increased transpiration (muted green) for shallow claypans because of increased soil water storage in the root zone. For claypans below the maximum rooting depth, transpiration decreased because of decreased water storage in the root zone and increased drainage from highly conductive sand below the maximum rooting depth (Fig. 14 and 15). The wider interquartile ranges of decreasing shifts in latent heat fluxes for claypans below the rooting depth correspond with the increased evaporative fractions (Fig. 10) and the losses in transpiration (Figs. 11 and 15); whereas, the opposite of these observations is true for claypans simulated above the maximum rooting depth except for 2013-SC80. The water balance for 2013-SC80 depicts transpiration losses for shallow claypans above the maximum rooting depth (Fig. 15) because of the reduced transpiration requirements of shallow rooting vegetation (Table 5) with increased precipitation.

All results from the Bronte simulations can be summarized as the following for an ustic soil moisture regime: 1) modeling with accurate texture properties did not produce significantly ($\alpha = 0.05$) different latent heat fluxes from homogeneous simulations (Fig. 7); 2) modeling soil profile textures heterogeneously with an abrupt contrast in coarseness will generate increased latent heat flux partitioning for shallow claypans (< 100 cm) and decreased latent heat flux partitioning for deep claypan interfaces (>100 cm) when

provided enough precipitation (Fig. 10, 11, and 14); 3) modeling the soil heterogeneously with an abrupt contrast in coarseness and shallower roots generated decreased latent heat fluxes for more summer days with increased latent heat flux partitioning where roots reach the claypan and decreased latent heat flux partitioning when the claypan is below the maximum rooting depth; 4) given a dryland climate experiencing decreased rainfall, shallow claypan simulations with an abrupt change in coarseness will enhance vegetation stress relative to claypans with milder changes in coarseness; and 5) given a dryland climate experiencing decreased rainfall, a sufficiently deep claypan simulation will reduce deep-rooting vegetation stress.

Discussion and Limitations

Modeling soil texture with vertical heterogeneity should improve the accuracy of predicting soil water content and its redistribution, but may not produce significant changes in surface heat partitioning for drier climates. Surface heat fluxes do change significantly for claypans with abrupt changes in texture and with different claypan depths. The changes in surface heat fluxes reflect the changes in soil water storage, redistribution, evapotranspiration, and plant available water. Therefore, claypans of varied depths have significant effects on the biophysical outputs. Because claypan depth is known to vary across a landscape, claypan soils can be expected to yield heterogenous biophysical outputs from spatial models, depending on simulated scale. The heat flux profiles created for this project provide a unique tool to potentially analyze the heterogeneity of landscape biophysical outputs by depicting how sensitive changes in a soil's texture depth are affecting the range and distribution of daytime latent heat fluxes.

This study deliberately limited several aspects of the RZWQM2 simulations to isolate the results strictly related to soil hydraulics. The intention of this study was to evaluate the effects of textural heterogeneity on mass and energy storage and redistribution at a fundamental level. As a result, the crop growth was modeled in a simplified fashion with the QuikTurf model. QuikTurf is a simple plant growth plug-in that maintains a zero-mass, constant rooting depth, while increasing leaf area index and plant height linearly to a maximum growth between turf trimming intervals. The plug-in does not compute stress and precipitation effects on vegetation growth so that RZWQM2 generates consistent responses to vegetation interacting with soil hydraulics.

CHAPTER IV

CONCLUSIONS

This study showed that simulating a heterogeneously textured soil profile outperformed the simulation of a homogeneously textured soil profile within the context of more accurately matching measurements of soil water content. Also, the partitioning of surface heat fluxes for a heterogeneously textured soil profile was shown to be significantly different compared to the simulation of a vertically homogeneous soil texture for a climate with sufficient rainfall to allow transpiration. Therefore, heterogeneous simulations of soil can cause sufficient changes to soil water storages and surface heat fluxes and, consequently, can alter simulation accuracy of the land-surface boundary condition. These differences in partitioning were pronounced in the climate with increased precipitation (Palestine, TX).

This study, also, demonstrated that a soil modeled with a claypan will have summertime daylight latent heat fluxes that change in a predictable manner based on the contrast of the surface texture and claypan texture, the profile's plant available water, the depth of the claypan, and the depth of the claypan with respect to rooting depth, such that:

1) the interquartile range of latent heat fluxes will shift to a maximum as the claypan interface deepens (> 5 cm) toward the maximum rooting depth;
2) if the maximum shift is reached before the maximum rooting depth, the shift will persist until the claypan interface depth and the maximum rooting depths

are the same, at which point, the interquartile range of latent heat fluxes will shift to a minimum;

3) the shift of the interquartile range will persist at the minimum until the claypan deepens sufficiently to reduce the effect of its matric potential on draining the overlying texture; and

4) sequentially deeper claypans below the rooting depth will increase the shift of latent heat flux interquartile ranges until water no longer drains from the overlying texture due to the claypan's matric potential.

Given non-drought conditions, large differences in textural coarseness between the surface soil and the claypan will widen the range of latent heat fluxes. Shallow rooting vegetation increases the difference between latent heat flux ranges generated from shallow claypans and deep claypans; whereas, deep rooting systems reduce this difference and produce more consistent heat flux ranges for claypans below about 20 cm.

Finally, this study has demonstrated that accurately representing vertical soil texture heterogeneity with depth significantly affects the soil water and surface heat fluxes that are important to modeling land-surface-atmosphere boundary condition. Furthermore, latent heat fluxes' inexorable tie to evapotranspiration, root water uptake, and plant available water implies that an abrupt change in a soil's subsurface texture can cause an abrupt and significant change in the latent heat fluxes exchanged at the land-surface-atmosphere boundary condition. Fortunately, soil textural heterogeneity information and average vegetation growths are available in the CONUS STATSGO for land surface models. Land surface modeling augmented with this readily available data may improve

estimations of weather and climate change tracking and predictions of atmospheric models.

There are further studies on the effect of soil vertical heterogeneity on soil water and surface heat fluxes that could be done. One study could involve a spatial comparison between the range of latent heat fluxes of a 2D heterogeneous land surface and a simulated heat flux profile of that land surface. Another study, may involve the clarification or development of standard heat flux profiles for different soil series or soil mapping units, but this may prove difficult given the lack of detailed surface heat flux data for specific land uses.

REFERENCES

Ares, J. 1976. Dynamics of the root system of blue grama. J. Range Manag. 29: 208–213.

Bell, J.E., M. a. Palecki, C.B. Baker, W.G. Collins, J.H. Lawrimore, R.D. Leeper, M.E. Hall, J. Kochendorfer, T.P. Meyers, T. Wilson, and H.J. Diamond. 2013. U.S. climate reference network soil moisture and temperature observations. J. Hydrometeorol. 14: 977–988.

Bennett, N.D., B.F.W. Croke, G. Guariso, J.H.A. Guillaume, S.H. Hamilton, A.J. Jakeman, S. Marsili-Libelli, L.T.H. Newham, J.P. Norton, C. Perrin, S.A. Pierce, B. Robson, R. Seppelt, A.A. Voinov, B.D. Fath, and V. Andreassian. 2013. Characterising performance of environmental models. Environ. Model. Softw. 40: 1–20.

Blanco-Canqui, H., C.J. Gantzer, S.H. Anderson, E.E. Alberts, and F. Ghidey. 2002. Saturated hydraulic conductivity and its impact on simulated runoff for claypan soils. Soil Sci. Soc. Am. J. 66: 1596–1602.

Brooks, R.H., and A.T. Corey. 1964. Hydraulic properties of porous media. Fort Collins, Colorado.

Brutsaert, W. 1967. Some methods of calculating unsaturated permeability. Trans. ASAE 10: 400–404.

Chen, F., and J. Dudhia. 2001. Coupling an advanced land surface–hydrology model with the Penn State–NCAR MM5 modeling system. Part I: Model implementation and sensitivity. Mon. Weather Rev. 129: 569–585.

Childs, E.C., and N. Collis-George. 1950. The permeability of porous materials. Proc. R. Soc. A Math. Phys. Eng. Sci. 201: 392–405.

D. N. Moriasi, B. N. Wilson, K. R. Douglas-Mankin, J. G. Arnold, and P. H. Gowda. 2012. Hydrologic and water quality models: Use, calibration, and validation. Trans. ASABE 55: 1241–1247.

Diamond, H.J., T.R. Karl, M.A. Palecki, C.B. Baker, J.E. Bell, R.D. Leeper, D.R. Easterling, J.H. Lawrimore, T.P. Meyers, M.R. Helfert, G. Goodge, and P.W. Thorne. 2013. U.S. climate reference network after one decade of operations status and assessment. Bull. Am. Meteorol. Soc. 94: 485–498.

Doolittle, J.A., K.A. Sudduth, N.R. Kitchen, and S.J. Indorante. 1994. Estimating depth to claypans using electromagnetic induction methods. J. Soil Water Conserv. 49: 572–

575.

Fang, Q.-X., T.R. Green, L. Ma, R.H. Erskine, R.W. Malone, and L.R. Ahuja. 2010. Optimizing soil hydraulic parameters in RZWQM2 under fallow conditions. Soil Sci. Soc. Am. J. 74: 1897–1913.

Farahani, H.J., and L.R. Ahuja. 1996. Evapotranspiration modeling of partial canopy/residue-covered fields. Trans. ASAE 39: 2051–2064.

Flerchinger, G.N., and F.B. Pierson. 1991. Modeling plant canopy effects on variability of soil temperature and water. Agric. For. Meteorol. 56: 227–246.

Flerchinger, G.N., and K.E. Saxton. 1989. Simultaneous heat and water model of a freezing snow-residue-soil system I. Theory and development. Trans. ASAE 32: 565–571.

Fox, G.A., R. Malone, G.J. Sabbagh, and K. Rojas. 2004. Interrelationship of macropores and subsurface drainage for conservative tracer and pesticide transport. J. Environ. Qual. 33: 2281–2289.

Gochis, D.J., E.R. Vivoni, and C.J. Watts. 2010. The impact of soil depth on land surface energy and water fluxes in the north american monsoon region. J. Arid Environ. 74: 564–571.

Green, W.H., and G.A. Ampt. 1911. Studies on soil physics Part I - The flow of air and water through soils. J. Agric. Sci. 4: 1–24.

Gupta, S.C., and W.E. Larson. 1979. Estimating soil water retention characteristics from particle size distribution, organic matter percent, and bulk density. Water Resour. Res. 15: 1633–1635.

Hanson, J.D., L.R. Ahuja, M.D. Shaffer, K.W. Rojas, D.G. DeCoursey, H. Farahani, and K. Johnson. 1998. RZWQM: Simulating the effects of management on water quality and crop production. Agric. Syst. 57: 161–195.

Jamison, V.C., and J.F. Thornton. 1961. Water intake rates of a claypan soil from hydrograph analyses. J. Geophys. Res. 66: 1855–1860.

Jenny, H., and G.D. Smith. 1935. Colloid chemical aspects of claypan formation in soil profiles. Soil Sci. 39: 377–389.

Kishné, A.S., Y.T. Yimam, C.L.S. Morgan, and B.C. Dornblaser. 2017. Evaluation and improvement of the default soil hydraulic parameters for the NOAH land surface model. Geoderma 285: 247–259.

Lawrence, D.M., K.W. Oleson, M.G. Flanner, P.E. Thornton, S.C. Swenson, P.J. Lawrence, X. Zeng, Z.-L. Yang, S. Levis, K. Sakaguchi, G.B. Bonan, and A.G. Slater. 2011. Parameterization improvements and functional and structural advances in version 4 of the Community Land Model. J. Adv. Model. Earth Syst. 3: 1–27.

Luo, Y., R.S. Loomis, and T.C. Hsiao. 1992. Simulation of soil temperature in crops. Elsevier Sci. Publ. B.V 61: 23–38.

Ma, L., L.R. Ahuja, B.T. Nolan, R.W. Malone, T.J. Trout, and Z. Qi. 2012. Root zone water quality model (RZWQM2): Model use, calibration, and validation. Trans. ASABE 55: 1425–1446.

Ma, L., L.R. Ahuja, S.A. Saseendran, R.W. Malone, T.R. Green, B.T. Nolan, P.N.S. Bartling, G.N. Flerchinger, K.J. Boote, and G. Hoogenboom. 2011. A protocol for parameterization and calibration of RZWQM2 in field research. In: Ahuja, L.R and L. Ma, editors, Methods of Introducing System Models into Agricultural Research. ASA, CSSA, and SSSA, Madison, WI. p. 1–64.

Miller, D.A., and R.A. White. 1998. A conterminous United States multilayer soil characteristics dataset for regional climate and hydrology modeling. Earth Interact. 2: 1–26.

Moriasi, D.N., J.G. Arnold, M.W. Van Liew, R.L. Bingner, R.D. Harmel, and T.L. Veith. 2007. Model evaluation guidelines for systematic quantification of accuracy in watershed simulations. Trans. ASABE 50: 885–900.

Nash, J.E., and J.V. Sutcliffe. 1970. River flow forecasting through conceptual models Part I — A discussion of principles. J. Hydrol. 10: 282–290.

Niu, G.Y., Z.L. Yang, K.E. Mitchell, F. Chen, M.B. Ek, M. Barlage, A. Kumar, K. Manning, D. Niyogi, E. Rosero, M. Tewari, and Y. Xia. 2011. The community NOAH land surface model with multiparameterization options (NOAH-MP): 1. Model description and evaluation with local-scale measurements. J. Geophys. Res. Atmos. 116: 1–19.

Quiring, S.M., T.W. Ford, J.K. Wang, A. Khong, E. Harris, T. Lindgren, D.W. Goldberg, and Z. Li. 2015. The north american soil moisture database: Development and applications. Bull. Am. Meteorol. Soc. 97: 1441–1459

Rawls, W.J., D.L. Brakensiek, and K.E. Saxton. 1982. Estimation of soil water properties. Trans. ASAE 25: 1316–1320.

Rawls, W.J., D. Gimenez, and R. Grossman. 1998. Use of soil texture, bulk density, and slope of the water retention curve to predict saturated hydraulic conductivity. Trans. ASAE 41: 983–988.

Richards, L.A. 1931. Capillary conduction of liquids through porous mediums. Physics. 1: 318–333.

Saxton, K.E., and W.J. Rawls. 2006. Soil water characteristic estimates by texture and organic matter for hydrologic solutions. Soil Sci. Soc. Am. J. 70: 1569–1578.

Saxton, K.E., W.J. Rawls, J.S. Romberger, and R.I. Papendick. 1986. Estimating generalized soil-water characteristics from texture. Soil Sci. Soc. Am. J. 50: 1031–1036.

Saxton, K.E., and F.D. Whitaker. 1970. Hydrology of a claypan watershed. Missouri Agricultural Experiment Station, Columbia, MO.

Seyfried, M.S., L.E. Grant, E. Du, and K. Humes. 2005. Dielectric loss and calibration of the hydra probe soil water sensor. Vadose Zo. J. 4: 1070.

Smith, G.D. 1934. Experimental studies on the development of heavy claypans in soils. University of Missouri Agricultural Experiment Station Publications, Columbia, MO.

Soil Survey Staff. 2015. Web Soil Survey. USDA-NRCS. http://websoilsurvey.nrcs.usda.gov (accessed 10 May 2015).

Soil Survey Staff. 2006. Land resource regions and major land resource areas of the united states, the caribbean, and the pacific basin. US Gov. Print. Office, Washington, DC.

Soil Survey Staff. 2015. Official soil series descriptions. USDA-NRCS. http://soils.usda.gov/technical/classification/osd/index.html (accessed 10 May 2015).

Soil Survey Staff. 2014. Keys to soil taxonomy. 12th ed. USDA-NRCS. US Gov. Print. Office, Washington, DC.

Starks, P.J., G.C. Heathman, L.R. Ahuja, and L. Ma. 2003. Use of limited soil property data and modeling to estimate root zone soil water content. J. Hydrol. 272: 131–147.

van Bavel, C.H.M., and D.I. Hillel. 1976. Calculating potential and actual evaporation from a bare soil surface by simulation of concurrent flow of water and heat. Agric. Meteorol. 17: 453–476.

Willmott, C.J. 1981. On the validation of models. Phys. Geogr. 2: 184–194.